Large Extracellular Vesicles Induce Stronger Prion Infection in Cell Culture than Small Extracellular Vesicles.

Running Title: Extracellular Vesicles Transmit Prions.

Jakub Soukup[1,2], Tibor Moško[1], Sami Kereïche[3], and Karel Holada[1]

[1]Institute of Immunology and Microbiology, First Faculty of Medicine, Charles University, 128 00 Prague, Czech Republic

[2]Department of Genetics and Microbiology, Faculty of Science, Charles University, 128 44 Prague, Czech Republic

[3]Institute of Biology and Medical Genetics, First Faculty of Medicine, Charles University, 128 00 Prague, Czech Republic

Abstract:

Prions are responsible for a number of lethal neurodegenerative and transmissible diseases in humans and animals. Extracellular vesicles, especially small exosomes, have been extensively studied in connection with various diseases. In contrast, larger microvesicles are often overlooked. In this work, we compared the ability of large extracellular vesicles (lEVs) and small extracellular vesicles (sEVs) to spread prions in cell culture. We utilized two cell culture models of prion infection and isolated lEVs by 20,000 × g force and sEVs by 110,000 × g force. The lEV fraction was enriched in β-1 integrin with a vesicle size starting at 150 nm. The fraction of sEVs was depleted of β-1 integrin with a mean size of 79 nm. Both fractions were enriched in prion protein, but the lEVs contained a higher prion-converting activity. In addition, lEV infection led to stronger prion signals in both cell cultures, as detected by cell and western blotting. Our data suggest the importance of lEVs in the trafficking and spread of prions over extensively studied small EVs.

23 Keywords: Cell Culture, Extracellular Vesicles, Infection, Prion

24 Introduction:

25 Prion diseases, such as CJD in humans or scrapie and bovine spongiform encephalopathy in animals, are
26 connected with the accumulation of pathologically misfolded prion protein (PrP^{TSE}) in the brains of
27 affected individuals (1). Normal cellular prion protein (PrP^{C}) has various posttranslational modifications,
28 including two potential N-glycosylation sites, which can be recognized by western blotting as three
29 distinct bands (2, 3). PrP^{C} is localized on membranes by a C-terminal GPI anchor (4). Its structure contains
30 three alpha helixes and a short beta-sheet (5, 6). The misfolding of PrP^{C} into PrP^{TSE} can occur sporadically
31 with or without genetic predisposition (1), induced to PrP^{C} by contact with PrP^{TSE} (1). The beta-sheet
32 structure of PrP^{TSE} is resistant (PrPres) to digestion with proteinase K (PK) (7), which could be used to
33 track infection in organs or cell cultures. Prions are most likely transmitted horizontally between
34 individuals by the oral pathway (8). However, how exactly prions spread from the gut to the brain
35 remains unknown. One possible theory described by McBride et al. (9) is that prions could transmit via
36 splanchnic and vagus nerves. Other possible routes are through lymphoid tissue (10) and follicular
37 dendritic cells (11). Intercellular transmission occurs in three possible ways: 1) cell-to-cell contact (12), 2)
38 tunneling nanotubes (13), and 3) EVs (14). Other mechanisms have been proposed, such as trogocytosis
39 or GPI-painting (15, 16).

40 Extracellular vesicles (EVs) are small cell-derived lipid vesicles with significant physiological and
41 pathological functions (17). EVs can be divided into three primary groups depending on their size and
42 biogenesis. Exosomes are generated by endosomal sorting complex required for transport (ESCRT)-
43 dependent (18, 19) and ESCRT-independent pathways (20). The ESCRT-dependent pathway involves the
44 ESCRT mechanism, formed by four distinct heterotrimers (ESCRT-0, ESCRT-I, ESCRT-II, and ESCRT-III) of
45 inward budding in early endosomes generating intraluminal vesicles (ILVs) and maturing early

46 endosomes in multivesicular bodies (MVBs) (18, 19). MVBs can be recycled back to the cell membrane,
47 releasing ILVs as exosomes with sizes of 30–100 nm (18, 21). Another pathway leads MVBs to fuse with
48 lysosomes, degrading ILVs (22, 23). Additionally, MVBs can fuse with autophagosomes, creating
49 amphisomes from which ILVs are released (24, 25). As a result, exosomes contain ESCRT-associated
50 proteins such as TSG-101, tetraspanins (CD9, CD63, CD81), or Alix (through the Syntenin-Alix pathway
51 (26, 27)). An ESCRT-independent pathway utilizes neutral sphingomyelinase (NSMase), which hydrolyzes
52 sphingomyelin to ceramide and induces the aggregation of microdomains to form ILVs (20).
53 Microvesicles (MVs) are vesicles 100–1000 nm in size (18) generated by direct budding from the cell
54 membrane. The budding of MVs is regulated by Cdc42 (a Rho family protein) and its downstream
55 effector Ras GTPase activating-like protein 1 (28). The actin cytoskeleton regulator RhoA is also involved
56 in the dynamics of MV budding (29, 30). ESCRT-I and III mechanisms play roles also in MV biogenesis.
57 Furthermore, ceramide has been reported to be involved in the biogenesis (31, 32). Cone shape-
58 structured tetraspanins are also involved in forming MVs (33). Based on their biogenesis, MVs contain
59 adhesion molecules such as β-1 integrin (34, 35) or Annexin A1 (36). The last primary type of
60 extracellular vesicles is apoptotic bodies, which have variable sizes between 50 and 5000 nm and are
61 generated during apoptosis (35). Apoptotic bodies are enriched with phosphatidylserine on their surface,
62 targeting it for fast phagocytosis by leukocytes (35), which should eliminate them from effective cellular
63 communication (37). Recently, more subpopulations of EVs have been distinguished using various
64 isolation techniques (27, 36, 38, 39).

65 In the cell, PrP^{C} is translocated to the plasma membrane in both nonraft (40) and raft domains (41-43),
66 where it is recycled back by clathrin- or caveolin-1-coated pits to endosomes, from which it can mature
67 into MVBs (40, 44-46). Cytosolic PrP^{C} is prevalent in MVBs (47, 48), with endolysosomal complexes
68 serving as one of the conversion sites for PrP^{TSE} (49, 50). Vilette et al. (51) found that exosomal prion
69 infectivity is associated with both ESCRT-dependent and ESCRT-independent release pathways. The

70 intercellular infectivity of PrP^{TSE} is decreased by blocking NSMase-2, while the PrP^{TSE} content in the cell
71 increases (48, 52). PrP^{TSE} present in exosomes (14) is able to infect neuronal cells both in vitro and in vivo
72 (53). One of the possible physiological roles of PrP^{C} is the mediation of EV transport along neuronal cells,
73 for which PrP^{C} located in EVs hydrophilically interacts with neuronal PrP^{C} located on the plasma
74 membrane (54), which is proposed to be the primary conversion site for PrP^{TSE} (49, 55). From the plasma
75 membrane, PrP^{TSE} is also transported via the endolysosomal pathway (56) to lysosomes (57) and possibly
76 MVBs. As exosomes, PrP^{TSE} on membrane-derived microvesicles is also released from cells (58).

77 PrP^{TSE} is present in plasma EVs of symptomatic and asymptomatic mice infected with prions (59, 60).
78 Thus, via blood transfusion, EVs can contribute to recorded horizontal infection with variant CJD (61).
79 The involvement of EVs in the oral pathway of infection is also possible since EVs can survive the
80 stomach environment (62, 63).

81 In our work, we utilized two cell culture models of prion infection to compare PrP^{TSE} content and prion
82 infectivity in the sEV fraction predominant with exosomes and the lEV fraction predominant with
83 microvesicles. Here, we report that both fractions of EVs are enriched in PrP, but lEVs are able to infect
84 native cells with more efficiency than sEVs.

85 Methods:

86 Materials:

87 Antibodies: From Abcam, we obtained rabbit anti-β-actin (EPR21241), fin. con. 0.25 µg/ml; and mouse
88 anti-Alix (3A9), fin. con. 2 µg/ml. From Azure Biosystems, we obtained goat anti-mouse AzureSpectra 700
89 or 800 conjugate, fin. con. 0.4 µg/ml; and goat anti-rabbit AzureSpectra IR700 or IR800 conjugate, fin.
90 con. 0.4 µg/ml. From Enzo Life Sciences, we obtained rabbit anti-HSP70/HSC70 (ADI-SPA-797), fin. con. 1
91 µg/ml; and rabbit anti-calnexin (ADI-SPA-865), fin. con. 1 µg/ml. From Santa Cruz Biotechnology, we

92 obtained rabbit anti-β1 integrin (M-106), fin. con. 2 µg/ml; goat anti-TSG-101 (M-19), fin. con. 2 µg/ml;
93 and rabbit anti-CD63 (H-193), fin. con. 2 µg/ml. Mouse anti-PrP (6D11), fin. con. 0.5 µg/ml was obtained
94 from Biolegend, mouse anti-CD9 (MM2/57), fin. con. 0.5 µg/ml was obtained from Merck; mouse anti-
95 PrP (AH6), fin. con. 0.5 µg/ml was obtained from The Roslin Institute, and donkey anti-mouse Alkaline
96 Phosphatase conjugate, fin. con. 0.3 µg/ml was obtained from Jackson ImmunoResearch.

97 ## Cells:

98 Prion infection models were used in the CAD5 cell line (originated from: RRID:CVCL_0199)(64), the N2a-
99 PK1 cell line (RRID:CVCL_WI10)(65), and cells chronically infected with the RML5 prion strain (CAD5-RML,
100 N2a-PK1-RML). The cells were maintained in Opti-MEM (Thermo Fisher Scientific) supplemented with
101 10% bovine growth serum (BGS, HyClone Bovine Growth Serum, GE Healthcare Life Sciences) and 100 U
102 of penicillin/streptomycin/ml (Lonza). CAD5 cells were passaged by washing with 0.5 mM EDTA in PBS
103 followed by resuspension in fresh medium. The N2a-PK1 cell line was passaged by washing with 0.5 mM
104 EDTA in PBS and trypsinized (Trypsin-EDTA 0.25%, Thermo Fisher Scientific).

105 All relevant data on EV production, isolation, and characterization were submitted to the EV-TRACK
106 knowledgebase (EV-TRACK ID: EV220318)(66). For EV production, the cells were passaged a day before
107 production (~ 30% confluence). Cells were washed with PBS (Lonza), and Exo-free Opti-MEM was added
108 for conditioning with EVs. The exo-free Opti-MEM medium was produced as published (67). Opti-MEM
109 supplemented with 20% BGS and penicillin/streptomycin was centrifuged at 110,000 × g (SW28 rotor,
110 Beckman) for 20 hours at 4 °C in an ultracentrifuge (LE-80K, Beckman). The centrifuged medium was
111 diluted with serum-free Opti-MEM supplemented with penicillin/streptomycin to a final concentration of
112 10% BGS and filtered using the Stericup-VP Sterile Vacuum Filtration System with a 0.1 µM PES filter
113 (Merck). The cells were incubated with the medium for 48 hours. When the conditioned medium was
114 harvested, the cells had 100% confluence with a minimum of dead/floating cells.

115 ## Isolation of EVs:

116 EVs were isolated from the conditioned medium by a series of differential centrifugations. All steps were
117 performed on ice, and samples were centrifuged at 4 °C. The conditioned medium was centrifuged at
118 300 × g for 15 min. The supernatant was collected and centrifuged at 2,000 × g for 20 min to sediment
119 large cell debris. The supernatant was centrifuged at 10,500 rpm (~20,000 × g) for 70 min (SW28 rotor,
120 Beckman). Pelleted lEVs were resuspended in 13.5 ml of PBS (Lonza) and sedimented again at 10,500
121 rpm (~20,000 × g) for 70 min (SW40 rotor, Beckman). The supernatant containing sEVs was centrifuged
122 at 25,000 rpm (~ 110,000 × g) for 70 min (SW28 rotor). The pellet was resuspended in ~ 12 ml of PBS and
123 underlaid with 2 ml of 40% sucrose in 0.2 M Tris-HCl pH 7.4 and centrifuged under the same conditions.
124 The sucrose cushion containing sEVs was collected with an 18 G needle, diluted with PBS to a final
125 volume of 13.5 ml, and centrifuged again. Both lEVs and sEVs were resuspended in PBS and frozen on dry
126 ice. Pure EVs were used for western blot characterization and infection using fractions standardized to
127 the same amount of protein determined by the BCA assay (Pierce BCA assay kit, Thermo Fisher
128 Scientific). The graphical scheme of isolation is shown in Fig. Extended View 1.

129 ## Infection of cells:

130 Native cells were passaged 24 h before infection. The cells were washed with 5 ml of PBS, and an Exo-
131 free medium containing isolated EVs was added for ~ 72 h. Two schemes of cell infection were used. In
132 the first scheme, lEVs and sEVs were standardized according to the original volume of the collected
133 sample. We abbreviated this scheme as OVS (Original Volume Standardization). The pelleted lEVs after
134 the first 20,000 × g spin and sEVs after the first 110,000 × g spin were resuspended in a volume of Exo-
135 free medium that was identical to the starting volume of the collected conditioned medium (8 ml).
136 Aliquots of 4, 2, and 1 ml were used to infect native cells in a 25 cm^2 flask or 100 µl in a 96-well plate. The
137 second infection scheme was standardized to contain the same amount of total protein used to infect
138 cells. We use TPS (Total Protein Standardization) as an abbreviation. Cells in a 25 cm^2 flask were infected

139 with 10, 5, or 2.5 µg of total protein in EV fractions. On a 96-well plate, the cells were infected with 0.2,
140 0.1, or 0.05 µg of EV fractions. The cells were passaged every 3-4 days to reach the 10th or 12th passage.
141 Two independent experiments, including EV production and isolation, were carried out. As a positive
142 control, the cell homogenates of RML-infected cells were used, and negative controls were homogenates
143 of the noninfected cells. The graphical scheme of infection is shown in Fig. Extended View 1.

144 **Extended View Figure 1: Scheme of lEV and sEV isolation and infection of native cells by the OVS and TPS.**

145 Harvesting of the cells after the infection for analysis:

146 CAD5 or CAD5-RML cells were resuspended in 0.5 mM EDTA in PBS by pipetting. N2a-PK1 or N2a-PK1-
147 RML cells were washed in 0.5 mM EDTA in PBS. The cells were centrifuged at 300 × g and 4 °C for 10 min,
148 the supernatant was discarded, and the pellets were frozen at -80 °C. The pellets were thawed on ice,
149 and freeze–thaw cycles were performed 3 times in total. The cells were homogenized using a 30 G
150 needle. To determine the protein concentration, part of the homogenate was lysed in lysis buffer (150
151 mM NaCl, 50 mM Tris-HCl pH 7.5, 0.5% (V/V) Triton X-100, 0.5% (w/V) sodium deoxycholate) along with
152 part of the collected EVs. The samples were incubated on ice for 30 min with occasional vortexing and
153 then centrifuged at 14,000 × g and 4 °C for 10 min. The supernatant was used to determine the protein
154 concentration by BCA assay according to the manufacturer's instructions (Pierce BCA Protein Assay Kit,
155 Thermo Fisher Scientific).

156 Cell blot:

157 All steps were performed at room temperature unless stated otherwise. Infected cells were seeded in
158 duplicate on a plastic coverslip in a 24-well plate and grown to confluency, as we published previously
159 (68). The coverslips were blotted on a 0.45 µm nitrocellulose membrane (Bio-Rad) wetted in lysis buffer.
160 The membranes were dried and incubated in lysis buffer containing 7 µg/ml proteinase K (PK, Sigma–
161 Aldrich) at 37 °C for 90 min. The membranes were washed 2× in Milli-Q H_2O (MQH_2O). The PK was
162 stopped with 2 mM phenylmethylsulfonyl fluoride (PMSF) in PBS for 10 min and washed 3× in MQH_2O.

163 The membranes were denatured with 3 M guanidium thiocyanate in 10 mM Tris-HCl pH 7.5 for 10 min
164 and washed with MQH_2O 5×. After denaturation, membranes were blocked in 5% nonfat milk in 0.5%
165 Tween in Tris buffer pH 7.4 (TBS-T) for 30 min. The primary antibodies anti-PrP 6D11 and AH6 were
166 diluted in a blocking solution, and the membranes were incubated for 2 h at RT or overnight at 4 °C with
167 antibodies. Membranes were washed with TBS-T 3× 5 min and incubated in secondary antibody
168 conjugated to alkaline phosphatase diluted in blocking solution for 1 h. The membranes were washed
169 with TBS 5× 5 min and developed using BCIP/NTP (Merck). The reaction was stopped using MQH_2O.
170 Densitometry was evaluated in AzureSpot software (v.2.0, Azure Biosystems) on background-corrected
171 images. Data are presented as the mean with standard error of the mean (SEM).

172 SDS–PAGE and western blot:

173 The frozen cell pellets were thawed on ice, resuspended in lysis buffer, and incubated on ice for 30 min
174 with occasional vortexing. Lysed cells were centrifuged at 14,000 × g at 4 °C for 10 min. The collected
175 supernatant was used to measure protein concentration using the BCA assay (Pierce BCA Protein Assay
176 Kit, Thermo Fisher Scientific) according to the manufacturer's instructions. The EVs were thawed on ice,
177 and part was diluted in lysis buffer to measure protein concentration as in cell lysates. Nonlysed EVs
178 were diluted with MQH_2O to unify the protein concentration, and sample buffer was added (final
179 concentration: 0.5 M Tris-HCl pH 6.8, 4% SDS, 0.125% bromophenol blue, 12.5% glycerol). Cell lysates
180 were diluted with MQH_2O to standardize the protein concentration before adding the sample buffer. To
181 detect PrPres, lysates and EVs were incubated with PK (50 µg/ml) at 37 °C for 45 min prior to adding the
182 sample buffer. The samples were boiled at 95 °C for 10 min. Boiled samples were loaded on 10%
183 acrylamide/bisacrylamide gel (Bio-Rad) or TGX Stain-Free™ FastCast™ 12% acrylamide gel (Bio-Rad).
184 Proteins on gels were imaged in an Azure c600 imaging system according to the manufacturer's
185 instructions. Separated proteins on the gels were blotted on Amersham™ Hybond® low-fluorescence 0.2
186 µm PVDF membranes (Merck). The membranes were blocked using fluorescence blocking buffer (Azure

187 Biosystems) at RT for 30 min. Primary antibodies were diluted in blocking buffer and incubated at RT for
188 2 h or at 4 °C overnight on a rocker. The membranes were washed with IR washing buffer (Azure
189 Biosystems) 3× 5 min. Washed membranes were incubated with secondary antibody diluted in blocking
190 buffer at RT for 1 h. Secondary antibodies were washed 3× 5 min in IR washing buffer and 2× 5 min in
191 PBS. After drying, the membranes were imaged using the Azure c600 imaging system. Densitometry was
192 evaluated in AzureSpot 2.0 software using predefined 200-radius rolling ball background subtraction.
193 Data are presented as the mean with SEM.

194 Real-Time Quacking Induced Conversion (RT-QuIC):

195 The collected EV pellets were thawed on ice and homogenized with a 30 G needle, and the protein
196 content was measured by BCA assay. Homogenized cells and EVs were diluted to 3.2 µg/µl using PBS,
197 corresponding to 10% cell homogenate protein content. By decimal and quintuple dilutions, EVs and cell
198 homogenate were diluted to 10^{-6} – 10^{-9} and 10^{-5} – 3×10^{-11}, respectively, in PBS buffer containing 1× N-2
199 supplement (Gibco, Thermo Fisher Scientific) and 0.1% SDS and then analyzed by second-generation RT-
200 QuIC assay. All samples were run in quadruplicate in a Nunc™ MicroWell™ 96-Well Optical-Bottom Plate
201 (Thermo Fisher Scientific). Each well contained reaction mix (10 mM phosphate buffer, pH 7.4; 300 mM
202 NaCl; 10 µM thioflavin T (ThT); 1 mM EDTA; 0.002% SDS; and 0.1 mg/ml rSHa PrP (90–231)) and 2 µL of
203 sample in a volume of 100 µL. The reaction was carried out using the FLUOstar Omega plate reader
204 (BMG LABTECH GmbH), undergoing repeating shaking cycles of 60 s (700 rpm, double orbital) and 60 s of
205 rest for 60 h at 55 °C. Fluorescence was measured every 15 min. Each test was analyzed using Mars
206 software (BMG LABTECH GmbH) (69, 70).

207 Cell Scrapie Assay:

208 All steps were performed at room temperature unless stated otherwise, as previously published (71).
209 Infected CAD5 cells were seeded in ELISPOT plates (multiscreen 96-well filter plates with high protein-

210 binding Immobilon-P membrane, 0.45 µm, Millipore) activated with 70% ethanol. Ethanol was removed
211 by vacuum (Supelco), and the wells were washed 2× with PBS. Cells (1,000, 5,000, or 10,000 per well)
212 were transferred to the plates, immobilized on the membrane using a vacuum, and dried at 50 °C. The
213 dried plates were incubated with 60 µl of PK (2 µg/µl) in lysis buffer at 37 °C for 30 min. PMSF (2 mM)
214 was added in PBS to inhibit PK for 10 min. Cells were washed with PBS, and proteins were denatured
215 with 3 M guanidium thiocyanate in 10 mM Tris-HCl pH 7.5 for 10 min and washed 4× with PBS. The
216 membranes were blocked using Superblock™ solution (Thermo Fisher Scientific) for 1 h. After blocking,
217 the membranes were incubated with 6D11 primary antibody diluted in Superblock™ solution at 4 °C
218 overnight. The primary antibody was washed away 4× with TBS-T, and the membranes were incubated
219 with a secondary antibody conjugated with alkaline phosphatase diluted in Superblock™ solution for 1 h.
220 The secondary antibody was washed away 5× with TBS-T and developed with an AP Conjugate Substrate
221 Kit (Bio-Rad). Spots were quantified using a Nikon ELISPOT system and NIS-Elements AR software (v.
222 4.20). GraphPad Prism 5 (v. 5.03, GraphPad Software) was used for statistical analysis. Infections with
223 lEVs were compared to corresponding sEV infections using a two-tailed unpaired t test (data passed the
224 D'Agostino and Pearson omnibus normality test and the Shapiro–Wilk normality test). Data are
225 presented as the mean with SEM.

226 Electron Microscopy:

227 For transmission electron microscopy (TEM), EM grids (FCF200-Cu, Electron Microscopy Sciences) were
228 prepared as published (67, 72). Isolated EVs were diluted 10× in PBS. Grids were incubated for 20 min on
229 a 15 µl drop of EV suspension and transferred to a 50 µl drop of 4% formaldehyde in PBS for another 20
230 min. The fixed samples were washed on a 100 µl drop of PBS and fixed again on a 50 µl drop of 1%
231 glutaraldehyde in PBS (electron microscopy grade, Sigma–Aldrich) for 5 min. The grids were washed 8×
232 on a 100 µl drop of MQH_2O. Washed grids were contrasted on 25 µl drops of uranyl oxalate pH 7 for 5
233 min. Contrasted grids were transferred on 25 µl drops on ice of a mix of 4% uranyl acetate and 2%

234 methylcellulose (1:9) for 10 min. The mix was slowly removed with filter paper, and the grid was air-
235 dried. Cryo-TEM samples were prepared by plunge freezing (72, 73). The EV sample (3 µl) was applied to
236 Lacey carbon grids (LC-200 Cu, Electron Microscopy Sciences) covered with a perforated carbon film and
237 discharged for 40 s with a 5 mA current. Most of the sample was removed by blotting (~ 1 s), and the
238 sample was immediately plunged into liquid ethane kept at -183 °C. The grids were transferred without
239 reheating to a Gatan 626 cryo-specimen holder and imaged in a Tecnai G2 Sphera 20 transmission
240 electron microscope equipped with a LaB6 gun and a Gatan UltraScan 1000 slow-scan CCD camera. The
241 images were recorded at an accelerating voltage of 120 kV. All pictures were CTF-corrected and
242 bandpass filtered to suppress ice thickness and noise below 1 nm detail size.

243 Results:

244 Characterization of lEV and sEV fractions

245 The isolated fractions of lEVs and sEVs from CAD5-RML and N2a-PK1-RML cells differed in protein
246 composition (Figs. 1A and B). Common markers for EVs, Alix, HSP70, TSG-101, CD63, and CD9, were
247 present in both fractions of EVs. In contrast, we did not detect calnexin, a marker of contamination by
248 the endoplasmic reticulum, in our EV fractions. In the CAD5-RML lEV fraction, very weak bands were
249 detected by calnexin antibody (Fig. 1C). To distinguish lEVs from sEVs, we used β-1 integrin as a marker
250 (Fig. 1C). Large EVs, which should consist mainly of MVs generated by budding from the plasma
251 membrane, should be enriched in this marker compared to sEVs. In CAD5-RML cell line, we isolated sEVs
252 depleted of β-1 integrin (Fig. 1C), but sEVs from N2a-PK1-RML cell line were not completely depleted of
253 β-1 integrin (Fig. 1D). The sEV fractions were enriched in the tetraspanin markers CD9 and CD63, TSG-
254 101, and Alix compared to the lEVs in both cell lines. The presence of EVs in isolated fractions was
255 verified by electron microscopy. As shown in Figs. 1E and F, CAD5 lEVs and sEVs differed in size. The size
256 difference was also visible in the N2a-PK1 cell line (Figs. 1G and H), although in sEVs, the vesicles were

257 larger compared to CAD5 cell sEVs. In addition, we used cryo-electron microscopy to visualize the
258 ultrastructure of CAD5 lEVs and sEVs where lipid bilayers were visible (Fig. 1I-L). We found that the mean
259 size (n = 200) of sEVs was 79 nm (SEM ±3 nm). The largest vesicles in the sEV fraction were
260 approximately 150 nm in diameter. The sizes of the visible vesicles in the lEV fraction ranged from ~100
261 nm – ~500 nm. Larger vesicles were present but deformed due to the thickness of the ice or holes in the
262 perforated carbon film (Fig. 1I).

263 **Figure 1: Characterization of lEV and sEV fractions.**
264 A, B. An example images of the TGX Stain-Free™ SDS–PAGE protein profile of CAD5-RML (A) or N2a-PK1 (B) cell lysate, lEVs, and
265 sEVs with the loading of 3 µg or 10 µg of proteins in line. Arrows point to examples of protein profile differences between cell
266 lysate, lEVs, and sEVs.
267 C, D. An example of images of the detection of markers in the EV fraction from the CAD5-RML (C) or N2a-PK1-RML (D) cell line.
268 β-1 integrin: marker of lEVs; calnexin: endoplasmic reticulum marker – contamination of EV fractions; Alix, HSP-70, TSG-101,
269 CD63 and CD9: common markers for sEVs and lEVs.
270 E-G. An example images of EVs present in the lEV (E, G) and sEV (F, H) fractions isolated from CAD5 (E, F) or N2a-PK1 (G, H) cells
271 contrasted with uranyl oxalate. Bars: 200 nm.
272 I-L. Cryo-electron microscopy images of vesicles in lEV (I, J) and sEV (K, L) fractions from CAD5 cells. Bars: 200 nm.
273 For visualization purposes, all images were enhanced with brightness and contrast.

274 Large and small EVs are enriched in PrP^{C} and PrP^{res} content compared to intact cells.

275 We found that PrP in both EV fractions was greatly enriched compared to the whole-cell lysates of
276 corresponding cell lines (Figs. 2A-D). When PrPres was normalized to whole-cell lysate PrP PK- (PrP^{C} +
277 PrP^{Sc}), we found that in lEVs, there was approximately five times more PrP^{res} in CAD5-RML cells and
278 approximately 18 times more PrPres in N2a-PK1-RML cells. In sEVs, there were approximately 8 and 11
279 times more PrPres than in the cell lysates of CAD5-RML cells and N2a-PK1-RML cells, respectively. There
280 was approximately 5× less PrPres in whole-cell lysate compared to PrP PK- in CAD5-RML cells and
281 approximately 20× less in N2a-PK1 cells. While the amount of PrPres was slightly higher (1.5×) in lEVs
282 than in sEVs from N2a-PK1-RML cells, the amount of PrP^{res} in lEVs from CAD5-RML cells was slightly
283 lower than that in sEVs (Fig. 2E). Similar patterns were also recorded for the amounts of PrP PK- in the EV
284 fractions in the CAD5-RML and N2a-PK1-RML cell lines (Fig. 2F).

285 **Figure 2: western blot analysis of PrP levels in EV fractions.**
286 A-D. CAD5-RML (A, B) or N2a-PK1-RML (C, D) lEVs, sEVs, and whole-cell lysate were treated with proteinase K (PK+, A, C), and
287 PrPres was detected using a mix of prion antibodies 6D11 and AH6. Untreated (PK-) samples (B, D) demonstrated the presence
288 of total PrP (PrP^{C} + PrP^{Sc}). For visualization purposes, all images were enhanced with brightness and contrast.

E, F. Comparison of the relative densities of PrPres bands in lEVs, sEVs, and whole-cell lysate normalized to PrP PK- signal in whole-cell lysate from CAD5-RML (E) or N2a-PK1-RML (F) cells. Bars represent the mean with SEM of biological triplicates, each with technical triplicates (3 different protein loadings on gel – 6, 3, or 1.5 µg per line).

Large EVs have higher prion-converting activity than small EVs.

We used an endpoint dilution RT-QuIC assay to determine the prion-converting activity in the EV fractions standardized to contain the same amount of total protein. The seeding dose 50 (SD_{50}) of CAD5-RML lEVs was twenty times higher than that of sEVs (2×10^{-8} vs. 4×10^{-7}, Fig. 3E). Additionally, the maximum relative fluorescence at a 10^{-5} dilution was higher and the lag phase shorter in lEVs (163,000 and 390 min, Fig. 3A) than in sEVs (151,000 and 480 min, Fig. 3B). In N2a-PK1-RML cells, the difference was less convincing. In the first experiment, there was approximately 26× higher prion-converting activity in lEVs (SD_{50}: 3×10^{-9} vs. 8×10^{-8}) and the maximum relative fluorescence and lag phase of the 10^{-5} dilution were 184,000 and 570 min for lEVs and 119,000 and 855 min for sEVs, respectively (Fig. 3C and D). In the second experiment, no difference was recorded (SD_{50}: 3×10^{-9} vs. 3×10^{-9}) and the respective values were 152,000 and 735 in lEVs and 146,000 and 690 in sEVs of the 10^{-5} dilution. The numbers of positive wells in quadruplicate for each sample and dilution are summarized in Appendix Table 1.

Figure 3: Comparison of EV fractions' prion converting activity using endpoint dilution RT-QuIC assay.
A-D. Quintuple dilution series of CAD5-RML lEVs (A), CAD5-RML sEVs (B), N2a-PK1-RML lEVs (C), and N2a-PK1-RML sEVs (D). Each line in the graphs represents the mean value of the technical quadruplicate. Redline – threshold (mean plus 5× standard deviation from negative control). NC (purple line) – negative control (uninfected CAD5 or N2a-PK1 whole cell lysate at 10^{-5} dilution, corresponding to 0.001% cell homogenate).
E. Table with seeding dose 50 from two independent experiments. The value represents the highest dilution, where at least 2 out of 4 technical replicates gave positive results.

A fraction of lEVs is more effective in the infection of cultured cells than a fraction of sEVs.

After fraction characterization, we infected native CAD5 or N2a-PK1 cells with EVs isolated from the corresponding chronically infected cells. First, we infected native CAD5 cells with supernatants collected during EV isolation (Fig. Extended View 2) to monitor the loss of infectivity produced by individual centrifugation steps. Most of the infectivity was lost after pelleting floating cells (300 × g). The next visible loss of infectivity occurred after pelleting of the lEVs. Some infectivity remained in the conditioned medium even after pelleting sEVs (110,000 × g supernatant) as demonstrated by visible

320 infection of the cells after 10 passages (Fig. Extended View 2F). The results from supernatant infection
321 were in agreement with the infection with collected pellets during the isolation procedure (Fig. Extended
322 View 3). We compared cell blots of infected cells with lEVs and sEVs in passages 3, 5, 8, and 10 (Fig. 4A-
323 D). We found that lEVs infected native cells more effectively than sEVs in both cell lines. We used two
324 schemes of infection: an OVS (original volume standardization) reflects the total amount of prion
325 infectivity associated with the isolated EV fractions, and a TPS (total protein standardization) reflects the
326 concentration of prion infectivity present in the isolated EV fractions. The differences in cell blot by OVS
327 infections were uniform during the passages after infection of CAD5 cells. Infection by lEVs was 1.5× -
328 2.3× stronger (1.7×, 1.5×, 1.5× and 2.3× in passages 3, 5, 8, and 10, respectively, Figs. 4E - H). Similarly,
329 infection by lEVs was stronger in TPS infection. In earlier passages, the difference was smaller. In passage
330 3, lEV infection was 1.4× stronger, and in passage 5, it was 1.6× stronger. In later passages 8 and 10, the
331 infection was 4.1× stronger (Figs. 4E – H). In the N2a-PK1 cell model, stronger infection by lEVs was
332 confirmed. The OVS led to 1.4× - 1.7× stronger infection by lEVs (1.7×, 1.4×, 1.5× and 1.4× in passages 3,
333 5, 8, and 10). In the TPS scheme of infection, lEVs infected N2a-PK1 cells 1.2× more strongly in all
334 passages, except for passage 5, where the infection by lEVs was weaker than that by sEVs (Figs. 4E – H).
335 The absolute values of the measured densities are shown in Appendix Fig. S1.

336 **Extended view Figure 2: Representative cell blots from infection of CAD5 cells with supernatants collected during isolation**
337 **steps of EVs.**
338 A. Infection with whole conditioned medium.
339 B. Infection with supernatant after pelleting of dead cells (300 × g).
340 C. Infection with supernatant after pelleting cell debris and apoptotic bodies (1,500 × g).
341 D. Infection with supernatant after pelleting lEVs (20,000 × g).
342 E. Infection with supernatant after pelleting sEVs (110,000 × g).
343 F. Positive control made from CAD5-RML cell homogenate.
344 G. Negative control made from native CAD5 cell homogenate.
345 For visualization purposes, all images were enhanced with brightness and contrast.
346
347 **Extended view Figure 3: Representative cell blots from the infection of CAD5 cells with pellets obtained during EV isolation**
348 **steps.** The infection was performed according to the OVS scheme, and 4, 2, or 1 ml of suspension was used for infection. D, E,
349 and F are part of Fig. 4 and are shown here for comparison with other fractions.
350 A. Cells harvested after collection of conditioned medium, homogenized, and resuspended in fresh medium.
351 B. Pellet representing dead cells in conditioning medium (300 × g).
352 C. Pellet representing large debris and apoptotic bodies (1,500 × g).
353 D. Pelleted lEVs (20,000 × g).
354 E. Pelleted sEVs (110,000 × g).

355 F. Negative control. Harvested and homogenized native CAD5 cells.
356 For visualization purposes, all images were enhanced with brightness and contrast.
357
358 **Figure 4: Example images of cell blots from passages after infection with lEVs and sEVs with densitometry analysis.**
359 A-D. Example images of cell blots from infection of native CAD5 or N2a-PK1 cells infected with lEVs and sEVs in different
360 passages after infection. Cells were infected with 4 ml, 2 ml, and 1 ml of resuspended EVs in OVS infection or with 10 µg, 5 µg,
361 and 2.5 µg of EVs in TPS infection. NC – negative control, PC – positive control. Passages 3 (A), 5 (B), 8 (C), and 10 (D) after
362 infection. For visualization purposes, all images were enhanced with brightness and contrast.
363 E-H. Densitometry analysis of cell blots from different passages. Infection with lEVs was compared to the corresponding
364 infection with sEVs. Bars represent the fold change in the density of lEVs compared to sEVs. Passages 3 (E), 5 (F), 8 (G), and 10
365 (H) after infection.
366 After cell blot analysis, we confirmed the results with western blotting from each passage and infection
367 (Fig. 5 and Appendix Figs. S2 – S4). From the same samples, western blot analysis showed that infection
368 of CAD5 cells by lEVs was even stronger compared to cell blot analysis. With the OVS scheme, the PrPres
369 signal from lEV-infected CAD5 cells was 1.5× - 3.6× stronger then from sEV-infected CAD5 cells (1.5×,
370 3.6×, 3.2×, and 1.9× in passages 3, 5, 8, and 10, Fig. 5E and Appendix Figs. S2-4). TPS infection by lEVs in
371 CAD5 cells led to a much higher PrPres signal in the CAD5 cell model than infection with sEVs. The PrPres
372 signal reached its maximum (where the dilutions had minimal differences) in passage 8, but infection by
373 sEVs just started to appear (Fig. 5C). Within these limitations, we measured a 24.6× stronger PrPres
374 signal in passage 8. Since lEV infection reached its maximum and infection by sEVs continued to increase,
375 the difference dropped to 7.0× and 10.6× in passages 10 and 12, respectively (Appendix Fig. S4E). In the
376 N2a-PK1 cell line, the trend of stronger infection by lEVs was similar. Unlike CAD5 cells, differences in TPS
377 infection were smaller than in OVS infection in N2a-PK1 cells. TPS infection led to 1.4× - 1.8× stronger
378 PrPres signals in lEV-infected cells than in sEV-infected cells (Fig. 5E and Appendix Figs. S2-4). In earlier
379 passages of the OVS scheme of infection, the PrPres signal was 2.0× and 1.9× stronger in infections by
380 lEVs in passages 3 and 5, respectively (Appendix Figs. S2 - S4). Later passages after infection by lEVs
381 revealed a 4.8× stronger PrPres signal in passage 8 and a 3.0× stronger signal in passage 10 (Fig. 5E and
382 Appendix Fig. S4). The absolute density values for each sample are summarized in Appendix Figures S5
383 and S6. As controls, we compared the total PrP signal of non-digested PrP PK- samples in the same
384 manner as PrPres (Fig. 5F). Despite the different strengths of infection by lEVs and sEVs, cells infected by
385 both types of EVs retained similar levels of PrP PK-. The lowest PrP PK- the ratio of lEVs/sEVs (0.96×) was

386 in passage 5 with OVS of CAD5 cells (Appendix Fig. 3F). The highest ratio of 1.84× was in the 10th passage
387 with OVS of N2a-PK1 cells (Appendix Fig. 4F). As a loading control for PrP PK-, β-actin was used (Fig. 5G).
388 Relative densities of β-actin bands were similar or higher in samples infected with sEVs than with lEVs,
389 confirming that the higher PrPres signal was not caused by elevated protein load.

390 **Figure 5: western blot analysis of PrPres and PrPSc/PrPc signals in cells infected by lEV and sEV fractions at passage 8.**
391 A-D. An example images of western blots from infection of CAD5 (A, C) or N2a-PK1 (B, D) cells with lEVs and sEVs at passage 8
392 after infection. Cells were infected with 4 ml, 2 ml, and 1 ml of resuspended EVs in OVS infection (A, B) or with 10 µg, 5 µg, and
393 2.5 µg of washed EVs in TPS infection (C, D). PK+ - proteinase K digested samples. β-Actin was used as a loading control for PrP
394 PK- samples, which were also compared. Both PrP PK- and PrP PK+ samples are shown for a loading of 40 µg per line. NC –
395 negative control (mock infected cells), PC – positive control. For visualization purposes, all images were enhanced with
396 brightness and contrast.
397 E. Relative comparison of PrP signal in PrP PK+ samples by densitometry. Bars represent fold change in the density of lEVs
398 compared to the corresponding density in infection of sEVs. Bars show the mean with SEM value of relative differences between
399 lEV and sEV infections from a biological duplicate of EV isolation, a triplicate of infection, and a technical triplicate of sample
400 loading. * PrPres signal reached its maximum in lEV infection and in sEV, infection just started to appear. The quantification
401 precision is limited.
402 F. Relative comparison of PrP PK- densitometry.
403 G. Relative comparison of β-actin densitometry.
404
405 As another validation method, we used the standard scrapie cell assay (SSCA) to quantify infection for
406 CAD5 cells precisely. The infections were carried out in hexaplicates for two independent EV isolations
407 (Figs. 6 A, B, E, F, I, and J). In SSCA, dilutions in the TPS scheme reached their maximum level of infection
408 in passage 8. We found a significant difference in passage 5. The mean spot counts (± SEM) in the 0.2 µg
409 infection were 250 ± 20 spots for lEVs and 188 ± 18 spots for sEVs ($p = 0.0309$). At 0.1 µg, there were 206
410 ± 23 spots for lEVs and 113 ± 12 spots for sEVs ($p = 0.0016$) (Fig. 6G). The differences were insignificant in
411 passages 3 (Fig. 6C) and 8 (Fig. 6K). The mean spot counts (± SEM) for lEVs in passage 8 were 553 ± 18,
412 520 ± 16, and 353 ±34 for 0.2, 0.1, and 0.05 µg of total protein, respectively. In sEVs, infection yielded
413 452 ± 48 spots in 0.2 µg, 433 ± 37 in 0.1 µg, and 322 ± 52 in 0.05 µg infection. In the OVS infection, we
414 found significant differences in passage 3 (Fig. 6D) and passage 8 (Fig. 6L) but not in passage 5 (Fig. 6H).
415 The mean spot counts were 511 ± 56 for lEVs and 267 ± 69 for sEVs ($p = 0.0054$, Fig. 6L) for passage 8. In
416 passage 3, the mean spot counts were 163 ± 17 for lEVs and 76 ± 12 for sEVs ($p = 0.0004$, Fig. 6D).

417 **Figure 6: Scrapie cell assay of CAD5 cells infected with EVs.**

418 A, E, I. Example images of wells in the scrapie cell assay infected with the TPS scheme in passages 3 (A), 5 (E), and 8 (I). PC –
419 positive control (infection by CAD5-RML cell homogenate), NC – negative control (infection by CAD5 cell homogenate). A total of
420 1000 cells were transferred to each well.
421 B, F, J. Representative images of wells in the scrapie cell assay infected with the OVS scheme in passages 3 (B), 5 (F), and 8 (J). A
422 total of 10,000 cells were transferred to each well.
423 C, G, K. Spot count in each well of the scrapie cell assay (hexaplicates of infection from a duplicate of isolation) – TPS infection in
424 passage 3 (C), 5 (G), and 8 (K). Each circle represents the count in one well. The thick line represents the mean value with SEM,
425 statistical significance was determined using an unpaired t-test ***P < 0.001 **P < 0.01 *P < 0.05.
426 D, H, L. Spot count in each well of the scrapie cell assay in OVS infection at passage 3 (D), 5 (H), and 8 (L).
427 For visualization purposes, all images were enhanced with brightness and contrast.

428 Discussion:

429 The presence of infectious prion protein in exosomes was demonstrated by Février et al. (14), which is
430 consistent with cellular prion conversion sites in the endolysosomal compartment, including MVBs (49,
431 50). However, one of the conversion sites of prion protein is the plasma membrane (55), and Mattei et
432 al. (58) found PrP^{TSE} in microvesicles. PrP^{TSE} can be transmitted via EVs in cell culture (52). According to
433 Godsave et al. (74), approximately 50% of PrP^{TSE} is on the cell surface, 30% in invaginations, and only
434 approximately 20% in cellular vesicles in the infected hippocampus. Although the predominant location
435 of PrP^{TSE} is on the cellular surface, no one has compared microvesicles and exosomes in the spread of
436 infection. To address this issue, we used a CAD5 cell model of prion infection infected with the RML prion
437 strain. As a second cell line, we chose N2a-PK1 cells. Although both cell lines were selected for high prion
438 production, CAD5 was produced by targeted oncogenesis of mouse catecholaminergic cells (75), and
439 N2a-PK1 was derived from mouse neuroblastoma cells (65). We tested the isolation protocol for
440 microvesicles and exosomes to collect enriched fractions of these vesicles. According to the International
441 Society of Extracellular Vesicles (ISEV) nomenclature and its position paper (76), we describe our
442 collected fractions as large EVs, pelleted at 20,000 × g and enriched in β-1 integrin, possibly
443 predominated by microvesicles. The sEVs were pelleted at 110,000 × g and enriched in CD9, CD63, TSG-
444 101, and Alix. This fraction should be predominated by exosomes. Although we optimized the isolation
445 procedure, we could not isolate the pure sEV fraction without β-1 integrin, which is one of the markers
446 for microvesicles (35), but it was recently also found in exosomes as another possible microvesicle

447 marker (36). This would explain the presence of β-1 integrin in our sEV fraction. Recently, Annexin A1
448 was found to be a specific marker for microvesicles (36). We found enrichment of CD9 tetraspanin in
449 sEVs compared to lEVs, as published previously (77). Based on the detection of β-1 integrin in the lEV
450 fraction, enrichment of CD9 in the sEV fraction compared to the lEV fraction, and no calnexin
451 contamination, we believe that our lEV fraction is predominated by microvesicles and the sEV fraction by
452 exosomes.

453 When we compared the EV fraction to the whole-cell lysate, we found great enrichment of both PrP^{TSE}
454 and PrP^{C}. The fraction of lEVs from CAD5 cells could not be isolated without contamination by calnexin
455 under the various centrifugations we tried during isolation optimization. Typically, the presence of
456 calnexin signals contamination from other cellular compartments (76). In our lEV and sEV fractions, there
457 was not a 100 kDa band of calnexin but three somewhat smaller bands that appeared in cells during
458 apoptosis (78), visible only after immense overexposure of the membrane (three times longer exposure
459 of the membrane or stretching of the histogram from 16 bit to 12 bit). Therefore, we assume that
460 apoptotic bodies could cause this contamination since they overlap in size.

461 Isolated fractions of EVs could be normalized in two possible ways. By total lipid concentration (79) or
462 total protein concentrations. Since we looked at prion protein transmission, we normalized EVs to
463 protein concentration using the BCA assay. Measurement of particle number in two fractions distinct in
464 size, which are heterogeneous, is problematic. Counting particles of different sizes by resistive pulse
465 sensing (RPS) did not yield reliable results. A fixed pore size is needed for reproducible measurement, yet
466 lEVs require a large pore size (80), with which sEVs are not detected (81). For NTA, this method has a
467 high relative concentration error for beads of 400 nm (82). The minimum sizes for measuring vesicles are
468 70-90 nm by NTA and 70-100 nm by RPS (82). In our sEV fraction, we detected the smallest particles with
469 a size of 30 nm by cryo-TEM. Furthermore, processing software may induce artifacts since the two
470 fractions need different settings (82).

471 We isolated both fractions from the same source, a conditioned medium, allowing us to compare these
472 fractions in PrP levels directly. The PrP PK- levels in lEVs and sEVs were relatively the same in the CAD5-
473 RML model, but in the N2a-PK1-RML model, the PrP PK- levels were slightly higher in lEVs. When we
474 looked at PrPres levels in CAD5 EVs, they were higher in sEVs. The difference in N2a-PK1 EVs was in the
475 opposite direction; the levels of PrPres were higher in lEVs. Our RT-QuIC experiments revealed higher
476 conversion activity in lEVs than in sEVs from both cell lines.

477 Next, we examined the infectivity of EVs by infecting native cells. First, we collected supernatants and
478 pellets from all steps of the isolation protocol to map the distribution of prion infectivity in the CAD5
479 model. As expected, all the fractions contained the infectivity, including the fractions of isolated EVs. In
480 accord with their higher RT-QuIC conversion activity, the lEVs caused approximately four times higher
481 CAD5 cell infection than sEVs in our initial cell blot experiments. We specifically looked at the difference
482 between EVs by two distinct approaches. The OVS scheme aimed to evaluate the differences in the
483 production of EVs by cells. Large EVs and sEVs were isolated from the same number of cells, and we
484 omitted the washing steps to eliminate the loss of EVs as much as possible. The TPS scheme aimed to
485 explore differences in the concentration of prion infectivity in washed vesicles and possibly also in their
486 uptake by the cells. With both infection schemes, we obtained concurrent results demonstrating higher
487 infectivity of lEVs in the CAD5 model. To overcome the limitations of cell blotting developed with alkaline
488 phosphatase, which is prone to signal saturation, we utilized fluorescent western blotting with greater
489 linear range of signal detection. The differences were even higher than in the cell blot. To further
490 demonstrate stronger infection by lEVs, we utilized SSCA to count number of infected cells directly.
491 Interestingly, in SSCA, we reached the infection plateau earlier (between the 5th and 8th passages)
492 compared to the cell blot and western blot (8th – 10th passages). In the fifth passage, we had
493 significantly more spots in TPS infection by lEVs. In OVS infection, we had significantly more spots in the

494 3rd and 8th passages in infection by lEVs. The differences measured by SSCA were less dramatic, but
495 consistent with the results of the cell and western blot analysis.

496 To confirm stronger infection by lEVs in the CAD5 model, we similarly tested the infection by EVs in the
497 N2a-PK1 cell line. Infection by lEVs was also stronger than that by sEVs with both infection schemes. In
498 CAD5 models, it is interesting to note that the TPS scheme infection led to a greater difference between
499 lEVs and sEVs suggesting higher concentration of the infectivity in lEVs. However, in the N2a-PK1 model,
500 the TPS infection scheme led only to small difference suggesting similar concentration of infectivity in
501 large and small EVs. In comparison, OVS infection scheme resulted in larger differences indicating
502 enhanced production of lEVs by N2a-PK1 cells. To purify sEVs from aggregated PrP (also pelleted at
503 110,000 × g), we introduced a sucrose cushion in the isolation of sEVs (83). Without the sucrose cushion
504 step, the measurement would be biased by pelleted PrP aggregates. The effectiveness of the cells
505 infection by lEVs and sEVs could be affected also by differences in their uptake. Since it is problematic to
506 separate microvesicles and exosomes, there is limited knowledge of the uptake of different fractions of
507 EVs. EVs can function as ligands for the surface receptor or be internalized by phagocytosis,
508 macropinocytosis, caveolin-mediated endocytosis, clathrin-mediated endocytosis, lipid raft-mediated
509 endocytosis, or fusion with the plasma membrane (32).

510 The CAD5 cells infected with the OVS scheme had a greater difference between infection levels in lEVs
511 and sEVs compared to the TPS scheme. Conversely, in N2a-PK1 cells, the TPS scheme resulted in a higher
512 discrepancy between infection levels in lEVs and sEVs compared to the OVS scheme. One possible
513 explanation could be in the cell origin. CAD5 is derived from Cath.a cells and has lost the immortalizing
514 oncogene (75). Cath.a cells secrete dopamine and norepinephrine (84), and cells secreting hormones and
515 neurotransmitters are specialized for secreting EVs (32). Conversely, the N2a-PK1 cell line is derived from
516 neuroblastoma Neuro 2A cells that produce low levels of tyrosine hydroxylase and dopamine unless they
517 are differentiated (85). It could be possible that the release of EVs is also specific to the cell type. The

518 RK13 lines, which express PrP^{C} from sheep, mice, or voles infected by different prion strains, release
519 PrP^{TSE} in exosomes differently (86).

520 Conclusion:

521 Prion protein is enriched in both large and small EVs. CAD5-RML lEVs contain higher prion converting
522 activity and infect native CAD5 cells more strongly than sEVs. We confirmed these results using three
523 different methods and two approaches to infection, one assessing the concentration of infectivity in
524 isolated EVs, and the second reflecting the total amount of infectivity associated with the EV fractions.
525 For validation, we used the N2a-PK1-RML cell line, in which we also achieved stronger infection by lEVs.
526 If the higher prion converting activity of lEVs was the sole reason why the infection with lEVs was
527 stronger remains to be elucidated since there is limited knowledge of the differences upon uptake of
528 different fractions of EVs. Small EVs or exosomes have been extensively studied compared to
529 microvesicles, yet microvesicles could play significant roles in other diseases, such as cancer or cellular
530 communication and immunity. Our data suggest the importance of lEVs in the trafficking of prions, which
531 should be considered in future prion transmission studies.

532 Declarations:

533 Ethics approval and consent to participate: Do not apply.

534 Consent of Publication: All authors agreed to publish the study.

535 Availability of data and material: We have submitted all relevant data of our experiments to the EV-
536 TRACK knowledgebase (EV-TRACK ID: EV220318). The data are available at the BioImage Archive
537 repository (URL: https://www.ebi.ac.uk/biostudies/studies/S-BSST1019).

538 The authors declare no conflicts of interest.

539 The study was funded by Charles University projects GA UK 360216 and Cooperatio 207032-3 and The
540 project National Institute for Neurological Research (Program EXCELES, ID Project No. LX22NPO5107) -
541 Funded by the European Union – Next Generation EU.

542 Author Contributions: Conceptualization: Jakub Soukup, Methodology: Jakub Soukup, Cryo-electron
543 Microscopy: Sami Kereïche, Jakub Soukup, RT-QuIC: Tibor Moško, writing – original draft: Jakub Soukup,
544 writing – review and editing: Karel Holada, Sami Kereïche, Jakub Soukup, Funding: Jakub Soukup, Karel
545 Holada.

546 Acknowledgment: The authors thank Charles Weissmann from The Scripps Research Institute (FL, USA)
547 for providing the CAD5, Peter Klöhn from MRC Prion Unit (London, UK) for providing the N2a-PK1 cells,
548 the TSE Resource Centre (Roslin Institute, UK) for providing the AH6 antibody, and Adriano Aguzzi
549 (Institute of Neuropathology, University of Zurich, Switzerland) for kindly providing the RML5 scrapie
550 strain. The TEM was performed in the Vinicna Microscopy Core Facility co-financed by the Czech-
551 BioImaging large RI project LM2023050. Computational resources were supplied by the project "e-
552 Infrastruktura CZ" (e-INFRA LM2018140) provided within the program Projects of Large Research,
553 Development and Innovations Infrastructure.

554 References:

555 1. Colby DW, Prusiner SB. Prions. Cold Spring Harbor Perspectives in Biology. 2011;3(1).
556 2. Lawson VA, Collins SJ, Masters CL, Hill AF. Prion protein glycosylation. J Neurochem.
557 2005;93(4):793-801.
558 3. Kostelanska M, Freisleben J, Hanusova ZB, Mosko T, Vik R, Moravcova D, et al. Optimization of
559 the photodynamic inactivation of prions by a phthalocyanine photosensitizer: The crucial involvement of
560 singlet oxygen. J Biophotonics. 2019;12(8):13.
561 4. Stahl N, Borchelt DR, Hsiao K, Prusiner SB. Scrapie Prion Protein Contains a Phosphatidylinositol
562 Glycolipid. Cell. 1987;51(2):229-40.
563 5. Riek R, Wider G, Billeter M, Hornemann S, Glockshuber R, Wuthrich K. Prion protein NMR
564 structure and familial human spongiform encephalopathies. Proceedings of the National Academy of
565 Sciences of the United States of America. 1998;95(20):11667-72.

566 6. Zahn R, Liu AZ, Luhrs T, Riek R, von Schroetter C, Garcia FL, et al. NMR solution structure of the
567 human prion protein. Proceedings of the National Academy of Sciences of the United States of America.
568 2000;97(1):145-50.
569 7. McKinley MP, Bolton DC, Prusiner SB. A protease-resistant protein is a structural component of
570 the Scrapie prion. Cell. 1983;35(1):57-62.
571 8. Gough KC, Maddison BC. Prion transmission Prion excretion and occurrence in the environment.
572 Prion. 2010;4(4):275-82.
573 9. McBride PA, Schulz-Schaeffer WJ, Donaldson M, Bruce M, Diringer H, Kretzschmar HA, et al. Early
574 spread of scrapie from the gastrointestinal tract to the central nervous system involves autonomic fibers
575 of the splanchnic and vagus nerves. Journal of Virology. 2001;75(19):9320-7.
576 10. Glaysher BR, Mabbott NA. Role of the GALT in scrapie agent neuroinvasion from the intestine.
577 Journal of Immunology. 2007;178(6):3757-66.
578 11. Brown KL, Stewart K, Ritchie DL, Mabbott NA, Williams A, Fraser H, et al. Scrapie replication in
579 lymphoid tissues depends on prion protein-expressing follicular dendritic cells. Nature Medicine.
580 1999;5(11):1308-12.
581 12. Kanu N, Imokawa Y, Drechsel DN, Williamson RA, Birkett CR, Bostock CJ, et al. Transfer of scrapie
582 prion infectivity by cell contact in culture. Curr Biol. 2002;12(7):523-30.
583 13. Gousset K, Schiff E, Langevin C, Marijanovic Z, Caputo A, Browman DT, et al. Prions hijack
584 tunnelling nanotubes for intercellular spread. Nature Cell Biology. 2009;11(3):328-U232.
585 14. Fevrier B, Vilette D, Archer F, Loew D, Faigle W, Vidal M, et al. Cells release prions in association
586 with exosomes. Proceedings of the National Academy of Sciences of the United States of America.
587 2004;101(26):9683-8.
588 15. Natale G, Ferrucci M, Lazzeri G, Paparelli A, Fornai F. Transmission of prions within the gut and
589 toward the central nervous system. Prion. 2011;5(3):142-9.
590 16. Sigurdson CJ, Bartz JC, Glatzel M. Cellular and Molecular Mechanisms of Prion Disease. Annu Rev
591 Pathol. 2019;14:497-516.
592 17. van Niel G, Carter DRF, Clayton A, Lambert DW, Raposo G, Vader P. Challenges and directions in
593 studying cell-cell communication by extracellular vesicles. Nat Rev Mol Cell Biol. 2022;23(5):369-82.
594 18. Colombo M, Raposo G, Thery C. Biogenesis, Secretion, and Intercellular Interactions of Exosomes
595 and Other Extracellular Vesicles. In: Schekman R, Lehmann R, editors. Annual Review of Cell and
596 Developmental Biology, Vol 30. Annual Review of Cell and Developmental Biology. 30. Palo Alto: Annual
597 Reviews; 2014. p. 255-89.
598 19. Henne WM, Buchkovich NJ, Emr SD. The ESCRT Pathway. Dev Cell. 2011;21(1):77-91.
599 20. Trajkovic K, Hsu C, Chiantia S, Rajendran L, Wenzel D, Wieland F, et al. Ceramide triggers budding
600 of exosome vesicles into multivesicular Endosomes. Science. 2008;319(5867):1244-7.
601 21. Heijnen HFG, Schiel AE, Fijnheer R, Geuze HJ, Sixma JJ. Activated platelets release two types of
602 membrane vesicles: Microvesicles by surface shedding and exosomes derived from exocytosis of
603 multivesicular bodies and alpha-granules. Blood. 1999;94(11):3791-9.
604 22. Buschow SI, Nolte-'t Hoen ENM, van Niel G, Pols MS, ten Broeke T, Lauwen M, et al. MHC II in
605 Dendritic Cells is Targeted to Lysosomes or T Cell-Induced Exosomes Via Distinct Multivesicular Body
606 Pathways. Traffic. 2009;10(10):1528-42.
607 23. Klumperman J, Raposo G. The Complex Ultrastructure of the Endolysosomal System. Cold Spring
608 Harbor Perspectives in Biology. 2014;6(10):22.
609 24. Hessvik NP, verbye A, Brech A, Torgersen ML, Jakobsen IS, Sandvig K, et al. PIKfyve inhibition
610 increases exosome release and induces secretory autophagy. Cellular and Molecular Life Sciences.
611 2016;73(24):4717-37.
612 25. Murrow L, Malhotra R, Debnath J. ATG12-ATG3 interacts with Alix to promote basal autophagic
613 flux and late endosome function. Nature Cell Biology. 2015;17(3):300-+.

614 26. Baietti MF, Zhang Z, Mortier E, Melchior A, Degeest G, Geeraerts A, et al. Syndecan-syntenin-ALIX
615 regulates the biogenesis of exosomes. Nature Cell Biology. 2012;14(7):677-85.
616 27. Kowal J, Arras G, Colombo M, Jouve M, Morath JP, Primdal-Bengtson B, et al. Proteomic
617 comparison defines novel markers to characterize heterogeneous populations of extracellular vesicle
618 subtypes. Proceedings of the National Academy of Sciences of the United States of America.
619 2016;113(8):E968-E77.
620 28. Wang J, Zhuang XJ, Greene KS, Si H, Antonyak MA, Druso JE, et al. Cdc42 functions as a regulatory
621 node for tumour-derived microvesicle biogenesis. Journal of Extracellular Vesicles. 2021;10(3):17.
622 29. Dai HJ, Zhang SS, Du XK, Zhang WK, Jing R, Wang XX, et al. RhoA inhibitor suppresses the
623 production of microvesicles and rescues high ventilation induced lung injury. Int Immunopharmacol.
624 2019;72:74-81.
625 30. Sun MJ, Xue XF, Li LY, Xu DD, Li SH, Li SWC, et al. Ectosome biogenesis and release processes
626 observed by using live-cell dynamic imaging in mammalian glial cells. Quant Imaging Med Surg.
627 2021;11(11):4604-16.
628 31. Nabhan JF, Hu RX, Oh RS, Cohen SN, Lu Q. Formation and release of arrestin domain-containing
629 protein 1-mediated microvesicles (ARMMs) at plasma membrane by recruitment of TSG101 protein.
630 Proceedings of the National Academy of Sciences of the United States of America. 2012;109(11):4146-51.
631 32. van Niel G, D'Angelo G, Raposo G. Shedding light on the cell biology of extracellular vesicles. Nat
632 Rev Mol Cell Biol. 2018;19(4):213-28.
633 33. Andreu Z, Yanez-Mo M. Tetraspanins in extracellular vesicle formation and function. Front
634 Immunol. 2014;5:12.
635 34. Laghezza Masci V, Taddei AR, Gambellini G, Giorgi F, Fausto AM. Microvesicles shed from
636 fibroblasts act as metalloproteinase carriers in a 3-D collagen matrix. J Circ Biomark.
637 2016;5:1849454416663660.
638 35. Momen-Heravi F, Getting SJ, Moschos SA. Extracellular vesicles and their nucleic acids for
639 biomarker discovery. Pharmacol Ther. 2018;192:170-87.
640 36. Jeppesen DK, Fenix AM, Franklin JL, Higginbotham JN, Zhang Q, Zimmerman LJ, et al.
641 Reassessment of Exosome Composition. Cell. 2019;177(2):428-+.
642 37. Deleo AM, Ikezu T. Extracellular Vesicle Biology in Alzheimer's Disease and Related Tauopathy. J
643 Neuroimmune Pharm. 2018;13(3):292-308.
644 38. Bobrie A, Colombo M, Krumeich S, Raposo GA, Thery C. Diverse subpopulations of vesicles
645 secreted by different intracellular mechanisms are present in exosome preparations obtained by
646 differential ultracentrifugation. Journal of Extracellular Vesicles. 2012;1(1):11.
647 39. Zhang HY, Freitas D, Kim HS, Fabijanic K, Li Z, Chen HY, et al. Identification of distinct
648 nanoparticles and subsets of extracellular vesicles by asymmetric flow field-flow fractionation. Nature
649 Cell Biology. 2018;20(3):332-+.
650 40. Sunyach C, Jen A, Deng J, Fitzgerald KT, Frobert Y, Grassi J, et al. The mechanism of
651 internalization of glycosylphosphatidylinositol-anchored prion protein. Embo Journal. 2003;22(14):3591-
652 601.
653 41. Sarnataro D, Campana V, Paladino S, Stornaiuolo M, Nitsch L, Zurzolo C. PrPC association with
654 lipid rafts in the early secretory pathway stabilizes its cellular conformation. Molecular Biology of the
655 Cell. 2004;15(9):4031-42.
656 42. Fremuntova Z, Mosko T, Soukup J, Kucerova J, Kostelanska M, Hanusova ZB, et al. Changes in
657 cellular prion protein expression, processing and localisation during differentiation of the neuronal cell
658 line CAD 5. Biology of the Cell. 2020;112(1):1-21.
659 43. Brouckova A, Holada K. Cellular prion protein in blood platelets associates with both lipid rafts
660 and the cytoskeleton. Thromb Haemost. 2009;102(5):966-74.
661 44. Didonna A. Prion protein and its role in signal transduction. Cell Mol Biol Lett. 2013;18(2):209-30.

662 45. Shyng SL, Huber MT, Harris DA. A Prion Protien Cycles Between the Cell-surface and an Endocytic
663 Compartment in Cultured Neuroblastoma-Cells. Journal of Biological Chemistry. 1993;268(21):15922-8.
664 46. Peters PJ, Mironov A, Peretz D, van Donselaar E, Leclerc E, Erpel S, et al. Trafficking of prion
665 proteins through a caveolae-mediated endosomal pathway. J Cell Biol. 2003;162(4):703-17.
666 47. Yim YI, Park BC, Yadavalli R, Zhao XH, Eisenberg E, Greene LE. The multivesicular body is the
667 major internal site of prion conversion. J Cell Sci. 2015;128(7):1434-43.
668 48. Guo BB, Bellingham SA, Hill AF. The Neutral Sphingomyelinase Pathway Regulates Packaging of
669 the Prion Protein into Exosomes. Journal of Biological Chemistry. 2015;290(6):3455-67.
670 49. Veith NM, Plattner H, Stuermer CAO, Schulz-Schaeffer WJ, Burkle A. Immunolocalisation of PrPSc
671 in scrapie-infected N2a mouse neuroblastoma cells by light and electron microscopy. Eur J Cell Biol.
672 2009;88(1):45-63.
673 50. Marijanovic Z, Caputo A, Campana V, Zurzolo C. Identification of an Intracellular Site of Prion
674 Conversion. Plos Pathogens. 2009;5(5):15.
675 51. Vilette D, Laulagnier K, Huor A, Alais S, Simoes S, Maryse R, et al. Efficient inhibition of infectious
676 prions multiplication and release by targeting the exosomal pathway. Cellular and Molecular Life
677 Sciences. 2015;72(22):4409-27.
678 52. Guo BB, Bellingham SA, Hill AF. Stimulating the Release of Exosomes Increases the Intercellular
679 Transfer of Prions. Journal of Biological Chemistry. 2016;291(10):5128-37.
680 53. Vella LJ, Sharples RA, Lawson VA, Masters CL, Cappai R, Hill AF. Packaging of prions into
681 exosomes is associated with a novel pathway of PrP processing. Journal of Pathology. 2007;211(5):582-
682 90.
683 54. D'Arrigo G, Gabrielli M, Scaroni F, Swuec P, Amin L, Pegoraro A, et al. Astrocytes-derived
684 extracellular vesicles in motion at the neuron surface: Involvement of the prion protein. Journal of
685 Extracellular Vesicles. 2021;10(9):22.
686 55. Goold R, Rabbanian S, Sutton L, Andre R, Arora P, Moonga J, et al. Rapid cell-surface prion
687 protein conversion revealed using a novel cell system. Nat Commun. 2011;2.
688 56. Yamasaki T, Baron GS, Suzuki A, Hasebe R, Horiuchi M. Characterization of intracellular dynamics
689 of inoculated PrP-res and newly generated PrPSc during early stage prion infection in Neuro2a cells.
690 Virology. 2014;450:324-35.
691 57. Goold R, McKinnon C, Rabbanian S, Collinge J, Schiavo G, Tabrizi SJ. Alternative fates of newly
692 formed PrPSc upon prion conversion on the plasma membrane. J Cell Sci. 2013;126(16):3552-62.
693 58. Mattei V, Barenco MG, Tasciotti V, Garofalo T, Longo A, Boller K, et al. Paracrine Diffusion of PrPC
694 and Propagation of Prion Infectivity by Plasma Membrane-Derived Microvesicles. Plos One. 2009;4(4).
695 59. Saa P, Yakovleva O, de Castro J, Vasilyeva I, De Paoli SH, Simak J, et al. First Demonstration of
696 Transmissible Spongiform Encephalopathy-associated Prion Protein (PrPTSE) in Extracellular Vesicles
697 from Plasma of Mice Infected with Mouse-adapted Variant Creutzfeldt-Jakob Disease by in Vitro
698 Amplification. Journal of Biological Chemistry. 2014;289(42):29247-60.
699 60. Cervenakoya L, Saa P, Yakoyleva O, Vasilyeva I, de Castro J, Brown P, et al. Are prions transported
700 by plasma exosomes? Transfusion and Apheresis Science. 2016;55(1):70-83.
701 61. Saa P. Is sporadic Creutzfeldt-Jakob disease transfusion-transmissible? Transfusion.
702 2020;60(4):655-8.
703 62. Benmoussa A, Lee CHC, Laffont B, Savard P, Laugier J, Boilard E, et al. Commercial Dairy Cow Milk
704 microRNAs Resist Digestion under Simulated Gastrointestinal Tract Conditions. J Nutr.
705 2016;146(11):2206-15.
706 63. Rahman MM, Shimizu K, Yamauchi M, Takase H, Ugawa S, Okada A, et al. Acidification effects on
707 isolation of extracellular vesicles from bovine milk. Plos One. 2019;14(9):12.

708 64. Mahal SP, Baker CA, Demczyk CA, Smith EW, Julius C, Weissmann C. Prion strain discrimination in
709 cell culture: The cell panel assay. Proceedings of the National Academy of Sciences. 2007;104(52):20908-
710 13.
711 65. Klohn PC, Stoltze L, Flechsig E, Enari M, Weissmann C. A quantitative, highly sensitive cell-based
712 infectivity assay for mouse scrapie prions. Proceedings of the National Academy of Sciences of the
713 United States of America. 2003;100(20):11666-71.
714 66. Van Deun J, Mestdagh P, Agostinis P, Akay Ö, Anand S, Anckaert J, et al. EV-TRACK: transparent
715 reporting and centralizing knowledge in extracellular vesicle research. Nature Methods. 2017;14(3):228-
716 32.
717 67. Théry C, Amigorena S, Raposo G, Clayton A. Isolation and Characterization of Exosomes from Cell
718 Culture Supernatants and Biological Fluids. Current Protocols in Cell Biology. 2006;30(1):3.22.1-3..9.
719 68. Janouskova O, Rakusan J, Karaskova M, Holada K. Photodynamic inactivation of prions by
720 disulfonated hydroxyaluminium phthalocyanine. Journal of General Virology. 2012;93:2512-7.
721 69. Foutz A, Appleby BS, Hamlin C, Liu XQ, Yang S, Cohen Y, et al. Diagnostic and prognostic value of
722 human prion detection in cerebrospinal fluid. Ann Neurol. 2017;81(1):79-92.
723 70. Mosko T, Galuskova S, Matej R, Buzova M, Holada K. Detection of Prions in Brain Homogenates
724 and CSF Samples Using a Second-Generation RT-QuIC Assay: A Useful Tool for Retrospective Analysis of
725 Archived Samples. Pathogens. 2021;10(6):13.
726 71. Hanusova Z, Mosko T, Matej R, Holada K. Precision in the design of an experimental study
727 deflects the significance of proteinase-activated receptor 2 expression in scrapie-inoculated mice.
728 Journal of General Virology. 2017;98(6):1563-9.
729 72. Soukup J, Kostelanska M, Kereiche S, Hujacova A, Pavelcova M, Petrak J, et al. Flow Cytometry
730 Analysis of Blood Large Extracellular Vesicles in Patients with Multiple Sclerosis Experiencing Relapse of
731 the Disease. J Clin Med. 2022;11(10):15.
732 73. Dubochet J, Adrian M, Chang JJ, Homo JC, Lepault J, McDowall AW, et al. Cryo-electron
733 microscopy of vitrified specimens. Q Rev Biophys. 1988;21(2):129-228.
734 74. Godsave SF, Wille H, Pierson J, Prusiner SB, Peters PJ. Plasma membrane invaginations containing
735 clusters of full-length PrPSc are an early form of prion-associated neuropathology in vivo. Neurobiol
736 Aging. 2013;34(6):1621-31.
737 75. Qi YP, Wang JKT, McMillian M, Chikaraishi DM. Characterization of a CNS cell line, CAD, in which
738 morphological differentiation is initiated by serum deprivation. J Neurosci. 1997;17(4):1217-25.
739 76. Thery C, Witwer KW, Aikawa E, Alcaraz MJ, Anderson JD, Andriantsitohaina R, et al. Minimal
740 information for studies of extracellular vesicles 2018 (MISEV2018): a position statement of the
741 International Society for Extracellular Vesicles and update of the MISEV2014 guidelines. Journal of
742 Extracellular Vesicles. 2018;7(1):43.
743 77. Mathieu M, Nevo N, Jouve M, Valenzuela JI, Maurin M, Verweij FJ, et al. Specificities of exosome
744 versus small ectosome secretion revealed by live intracellular tracking of CD63 and CD9. Nat Commun.
745 2021;12(1):18.
746 78. Takizawa T, Tatematsu C, Watanabe K, Kato K, Nakanishi Y. Cleavage of calnexin caused by
747 apoptotic stimuli: Implication for the regulation of apoptosis. J Biochem(Tokyo). 2004;136(3):399-405.
748 79. Osteikoetxea X, Balogh A, Szabó-Taylor K, Németh A, Szabó TG, Pálóczi K, et al. Improved
749 Characterization of EV Preparations Based on Protein to Lipid Ratio and Lipid Properties. PLOS ONE.
750 2015;10(3):e0121184.
751 80. de Vrij J, Maas SL, van Nispen M, Sena-Esteves M, Limpens RW, Koster AJ, et al. Quantification of
752 nanosized extracellular membrane vesicles with scanning ion occlusion sensing. Nanomedicine (Lond).
753 2013;8(9):1443-58.

754 81. Coumans FAW, van der Pol E, Böing AN, Hajji N, Sturk G, van Leeuwen TG, et al. Reproducible
755 extracellular vesicle size and concentration determination with tunable resistive pulse sensing. Journal of
756 Extracellular Vesicles. 2014;3(1):25922.
757 82. van der Pol E, Coumans FA, Grootemaat AE, Gardiner C, Sargent IL, Harrison P, et al. Particle size
758 distribution of exosomes and microvesicles determined by transmission electron microscopy, flow
759 cytometry, nanoparticle tracking analysis, and resistive pulse sensing. J Thromb Haemost.
760 2014;12(7):1182-92.
761 83. Morales R, Hu PP, Duran-Aniotz C, Moda F, Diaz-Espinoza R, Chen B, et al. Strain-dependent
762 profile of misfolded prion protein aggregates. Sci Rep. 2016;6(1):20526.
763 84. Suri C, Fung BP, Tischler AS, Chikaraishi DM. Catecholaminergic cell lines from the brain and
764 adrenal glands of tyrosine hydroxylase-SV40 T antigen transgenic mice. J Neurosci. 1993;13(3):1280-91.
765 85. Tremblay RG, Sikorska M, Sandhu JK, Lanthier P, Ribecco-Lutkiewicz M, Bani-Yaghoub M.
766 Differentiation of mouse Neuro 2A cells into dopamine neurons. J Neurosci Methods. 2010;186(1):60-7.
767 86. Arellano-Anaya ZE, Huor A, Leblanc P, Lehmann S, Provansal M, Raposo G, et al. Prion strains are
768 differentially released through the exosomal pathway. Cellular and Molecular Life Sciences.
769 2015;72(6):1185-96.

770

771 **Appendix Figure S1: Absolute densities of cell blots after different passages after infection using EV fractions.**
772 A-D. Densities measured in passages 3 (A), 5 (B), 8 (C), and 10 (D). In OVS scheme, the cells were infected with 4 ml, 2 ml, and 1
773 ml of EVs resuspended in the original volume of medium and in TPS scheme with 10 µg, 5 µg, and 2.5 µg of washed EVs.
774 Duplicates 1 and 2 represent two independent experiments. Bars represent the mean value of two technical replicates.
775
776 **Appendix Figure S2: western blot analysis of PrPres and PrPSc/PrPc signals in cells infected by lEV and sEV fractions at**
777 **passage 3.**
778 A-D. An example images of western blots from infection of CAD5 (A, C) or N2a-PK1 (B, D) cells with lEVs and sEVs at passage 3
779 after infection. Cells were infected with 4 ml, 2 ml, and 1 ml of resuspended EVs in OVS infection (A, B) or with 10 µg, 5 µg, and
780 2.5 µg of washed EVs in TPS infection (C, D). PK+ - proteinase K digested samples. β-Actin was used as a loading control for PrP
781 PK- samples, which were also compared. Both PrP PK- and PrP PK+ samples are shown for a loading of 40 µg per line. NC –
782 negative control (mock infected cells), PC – positive control. For visualization purposes, all images were enhanced with
783 brightness and contrast.
784 E. Relative comparison of PrP signal in PrP PK+ samples by densitometry. Bars represent fold change in the density of lEVs
785 compared to the corresponding density in infection of sEVs. Bars show the mean with SEM value of relative differences between
786 lEV and sEV infections from a biological duplicate of EV isolation, a triplicate of infection, and a technical triplicate of sample
787 loading.
788 F. Relative comparison of PrP PK- densitometry.
789 G. Relative comparison of β-actin densitometry.
790
791 **Appendix Figure S3: western blot analysis of PrPres and PrPSc/PrPc signals in cells infected by lEV and sEV fractions at**
792 **passage 5.**
793 A-D. An example images of western blots from infection of CAD5 (A, C) or N2a-PK1 (B, D) cells with lEVs and sEVs at passage 5
794 after infection. Cells were infected with 4 ml, 2 ml, and 1 ml of resuspended EVs in OVS infection (A, B) or with 10 µg, 5 µg, and
795 2.5 µg of washed EVs in TPS infection (C, D). PK+ - proteinase K digested samples. β-Actin was used as a loading control for PrP
796 PK- samples, which were also compared. Both PrP PK- and PrP PK+ samples are shown for a loading of 40 µg per line. NC –
797 negative control (mock infected cells), PC – positive control. For visualization purposes, all images were enhanced with
798 brightness and contrast.
799 E. Relative comparison of PrP signal in PrP PK+ samples by densitometry. Bars represent fold change in the density of lEVs
800 compared to the corresponding density in infection of sEVs. Bars show the mean with SEM value of relative differences between
801 lEV and sEV infections from a biological duplicate of EV isolation, a triplicate of infection, and a technical triplicate of sample
802 loading.
803 F. Relative comparison of PrP PK- densitometry.
804 G. Relative comparison of β-actin densitometry.
805

806 **Appendix Figure S4: western blot analysis of PrPres and PrPSc/PrPc signals in cells infected by lEV and sEV fractions at**
807 **passage 10.**
808 A-D. An example images of western blots from infection of CAD5 (A, C) or N2a-PK1 (B, D) cells with lEVs and sEVs at passage 10
809 after infection (TPS infected CAD5 cells are shown in passage 12 after infection as the final passage). Cells were infected with 4
810 ml, 2 ml, and 1 ml of resuspended EVs in OVS infection (A, B) or with 10 µg, 5 µg, and 2.5 µg of washed EVs in TPS infection (C,
811 D). PK+ - proteinase K digested samples. β-Actin was used as a loading control for PrP PK- samples, which were also compared.
812 Both PrP PK- and PrP PK+ samples are shown for a loading of 40 µg per line. NC – negative control (mock infected cells), PC –
813 positive control. For visualization purposes, all images were enhanced with brightness and contrast.
814 E. Relative comparison of PrP signal in PrP PK+ samples by densitometry. Bars represent fold change in the density of lEVs
815 compared to the corresponding density in infection of sEVs. Bars show the mean with SEM value of relative differences between
816 lEV and sEV infections from a biological duplicate of EV isolation, a triplicate of infection, and a technical triplicate of sample
817 loading.
818 F. Relative comparison of PrP PK- densitometry.
819 G. Relative comparison of β-actin densitometry.
820
821 **Appendix Figure S5: Absolute PrPres densities of western blots of OVS-infected cells.**
822 A, B. Densities measured in passage 3, 5, 8, and 10 after infection of CAD5 (A) or N2a-PK1 (B) cells with EV fractions. The cells
823 were infected with 4 ml, 2 ml, and 1 ml of EVs resuspended in the original volume of the medium. Duplicates 1 and 2 represent
824 two independent experiments.
825 **Appendix Figure S6: Absolute PrPres densities of western blots of TPS-infected cells.**
826 A, B. Densities measured in passage 3, 5, 8, and 10 after infection of CAD5 (A) or N2a-PK1 (B) cells with EV fractions. The cells
827 were infected with 10 µg, 5 µg, and 2.5 µg of washed. Duplicates 1 and 2 represent two independent experiments.
828
829 **Appendix Table 1:** Summary of detection of prion converting activity in cell lysates from CAD5-RML or N2a-PK1-RML cells
830 (positive control) and isolated lEVs and sEVs from these cells. The negative control was cell lysate from CAD5 or N2a-PK1 cells.
831 Each sample was serially diluted in quadruplicate. The lowest dilution where at least two wells from quadruplicates (dark green)
832 marks the SD_{50}.

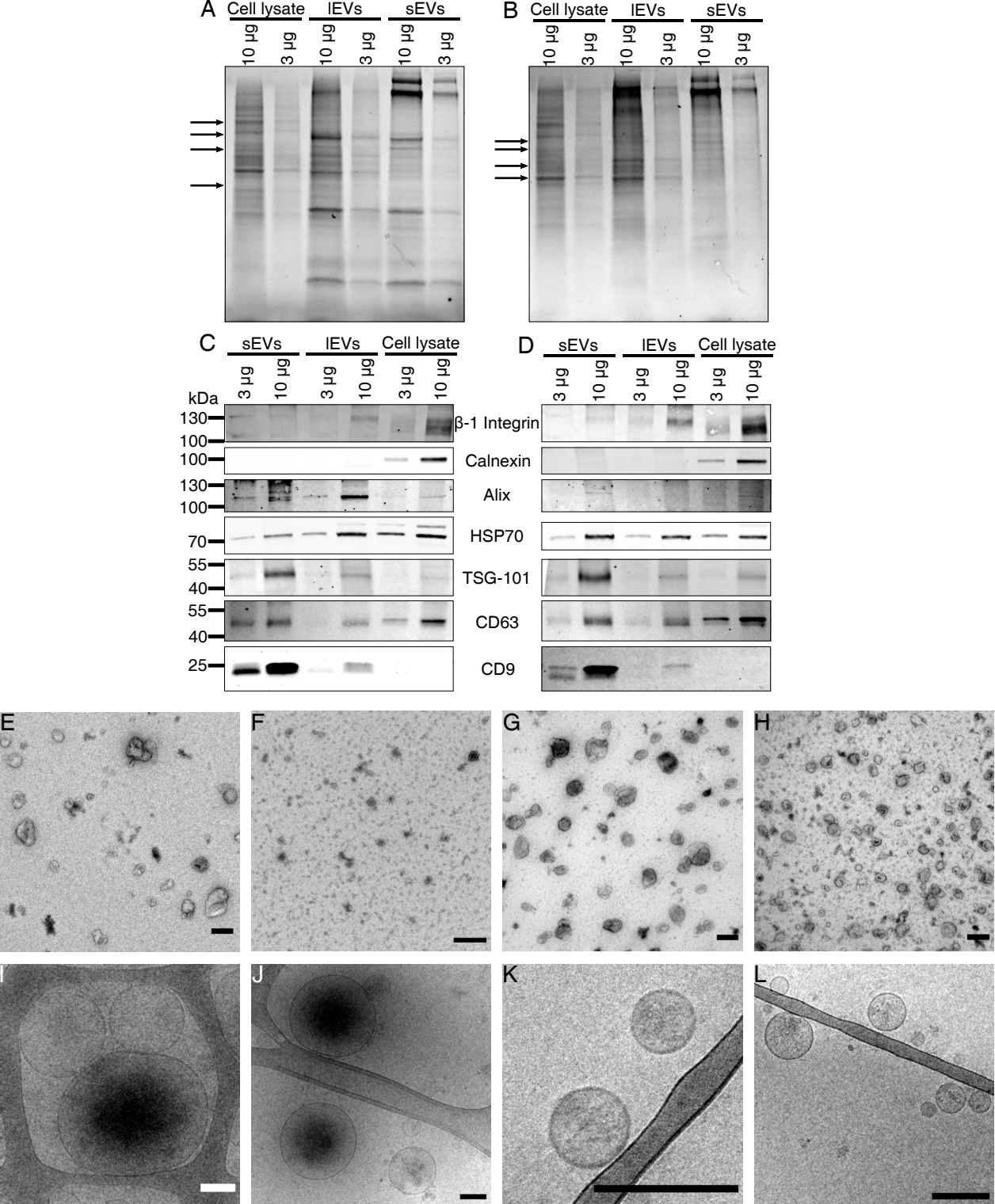
A
Cell lysate
lEVs
sEVs
10 µg
3 µg
B
C
D
kDa
130
100
70
55
40
25
β-1 Integrin
Calnexin
Alix
HSP70
TSG-101
CD63
CD9
E
F
G
H
I
J
K
L

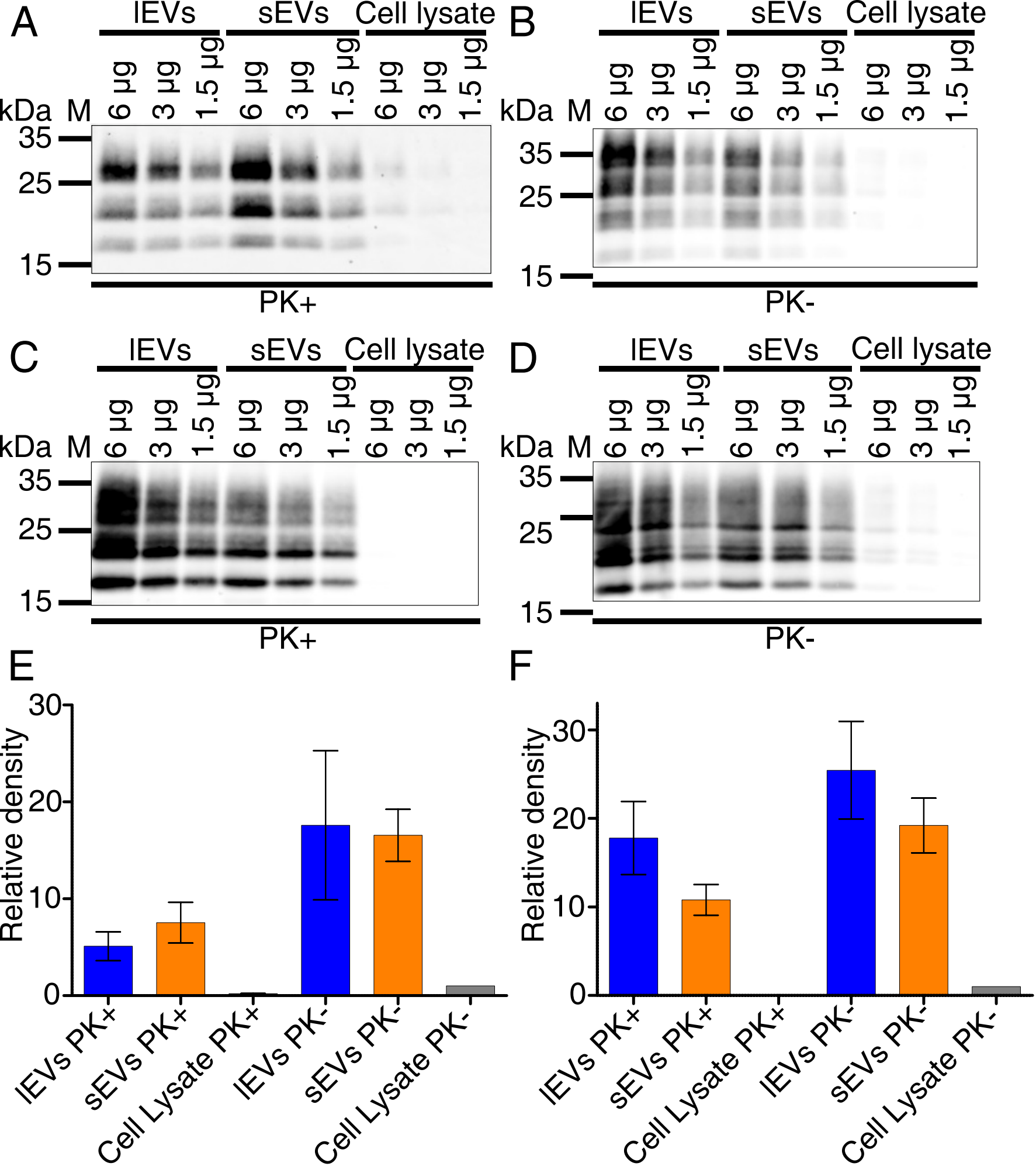
A
IEVs
sEVs
Cell lysate
6 µg
3 µg
1.5 µg
kDa
M
35
25
15
PK+
B
PK-
C
D
E
F
Relative density
30
20
10
0
IEVs PK+
sEVs PK+
Cell Lysate PK+
IEVs PK-
sEVs PK-
Cell Lysate PK-

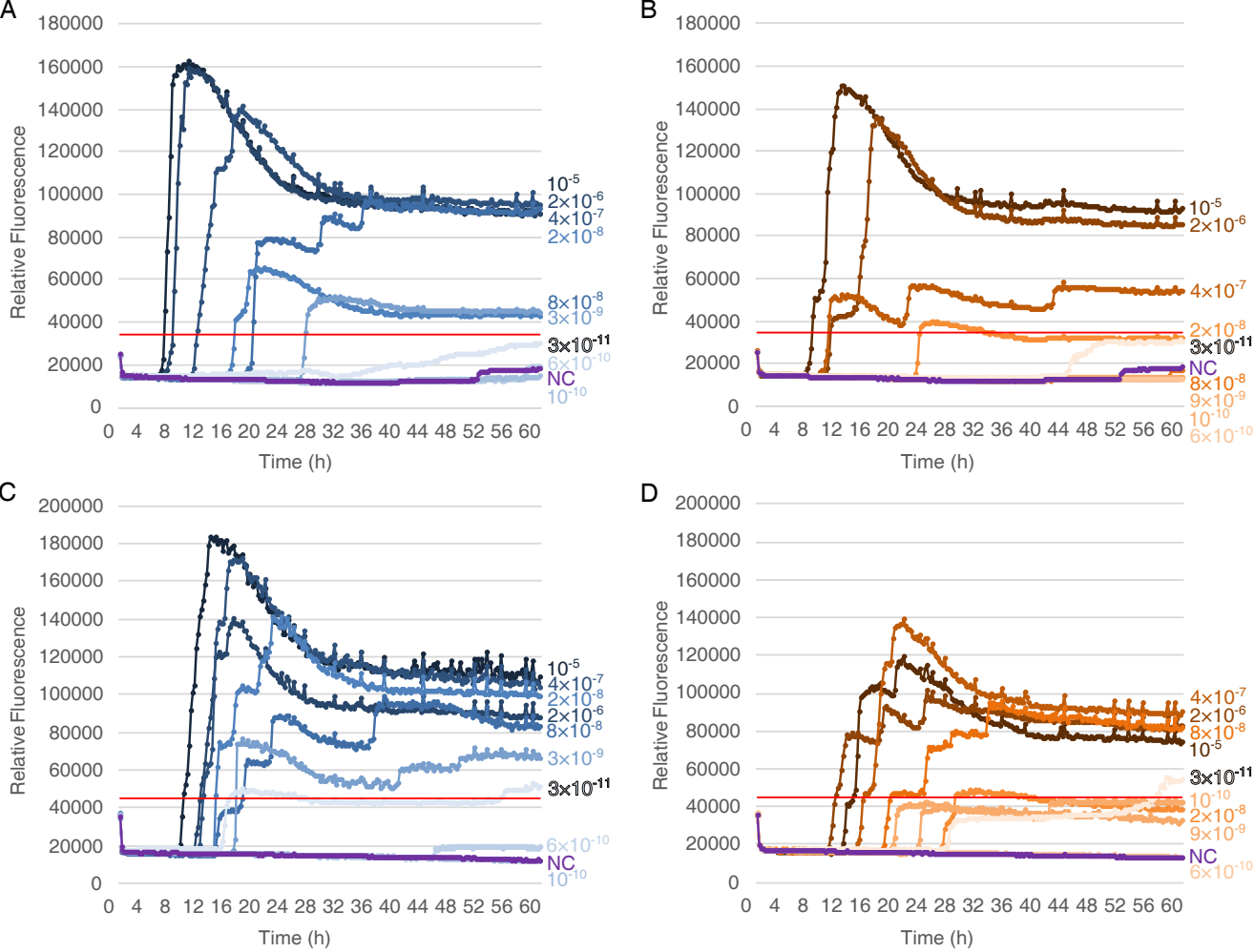

E

Seeding Dose 50			
Sapmle	lEVs	sEVs	Whole cell lysate
CAD5-RML 1st experiment	10^{-8}	10^{-6}	10^{-8}
CAD5-RML 2nd experiment	2×10^{-8}	4×10^{-7}	
PK1-N2a-RML 1st experiment	3×10^{-9}	3×10^{-9}	
PK1-N2a-RML 2nd experiment	3×10^{-9}	8×10^{-8}	

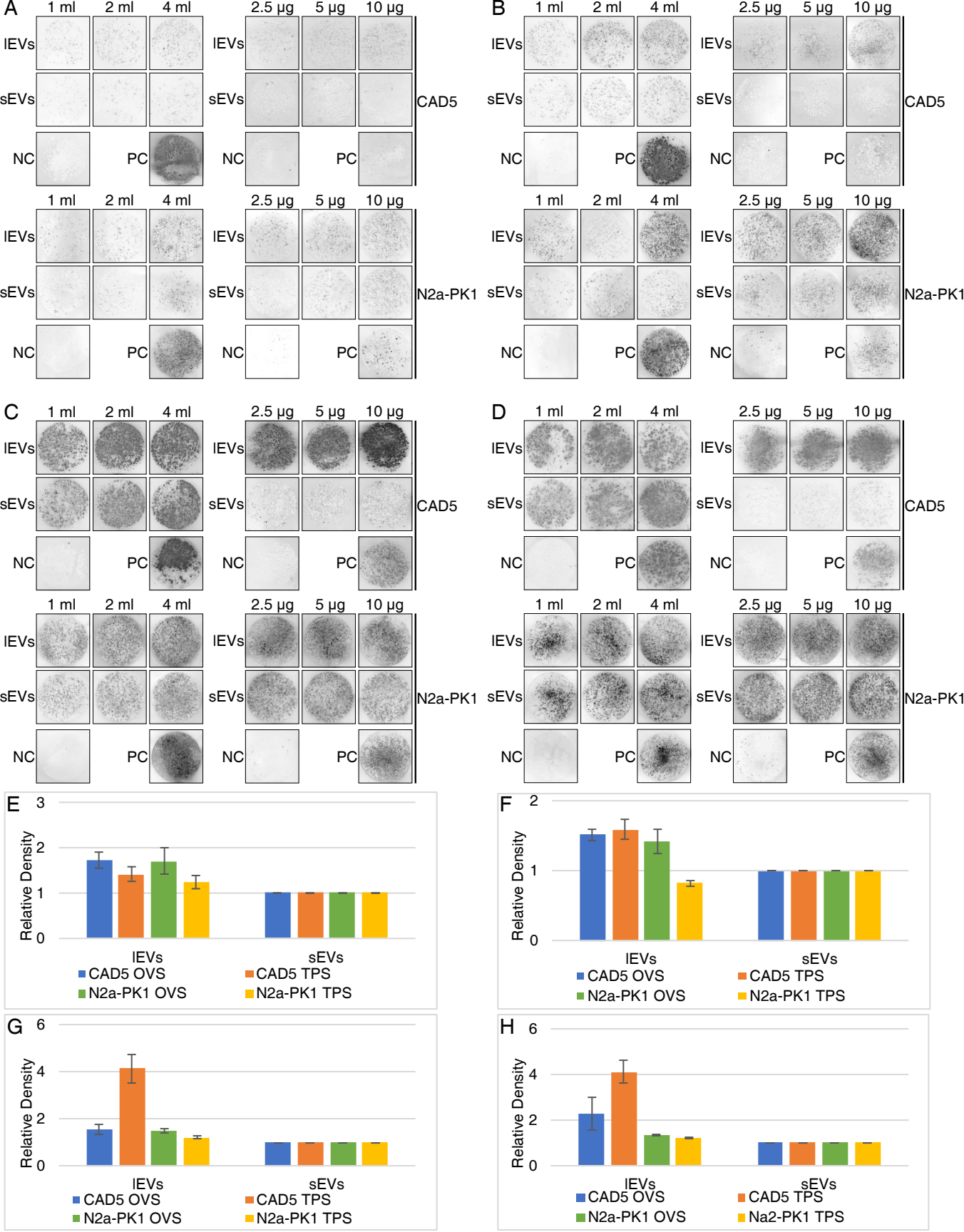
A
B
C
D
1 ml
2 ml
4 ml
2.5 µg
5 µg
10 µg
IEVs
sEVs
NC
PC
CAD5
N2a-PK1
E
F
G
H
Relative Density
IEVs
sEVs
CAD5 OVS
CAD5 TPS
N2a-PK1 OVS
N2a-PK1 TPS
Na2-PK1 TPS

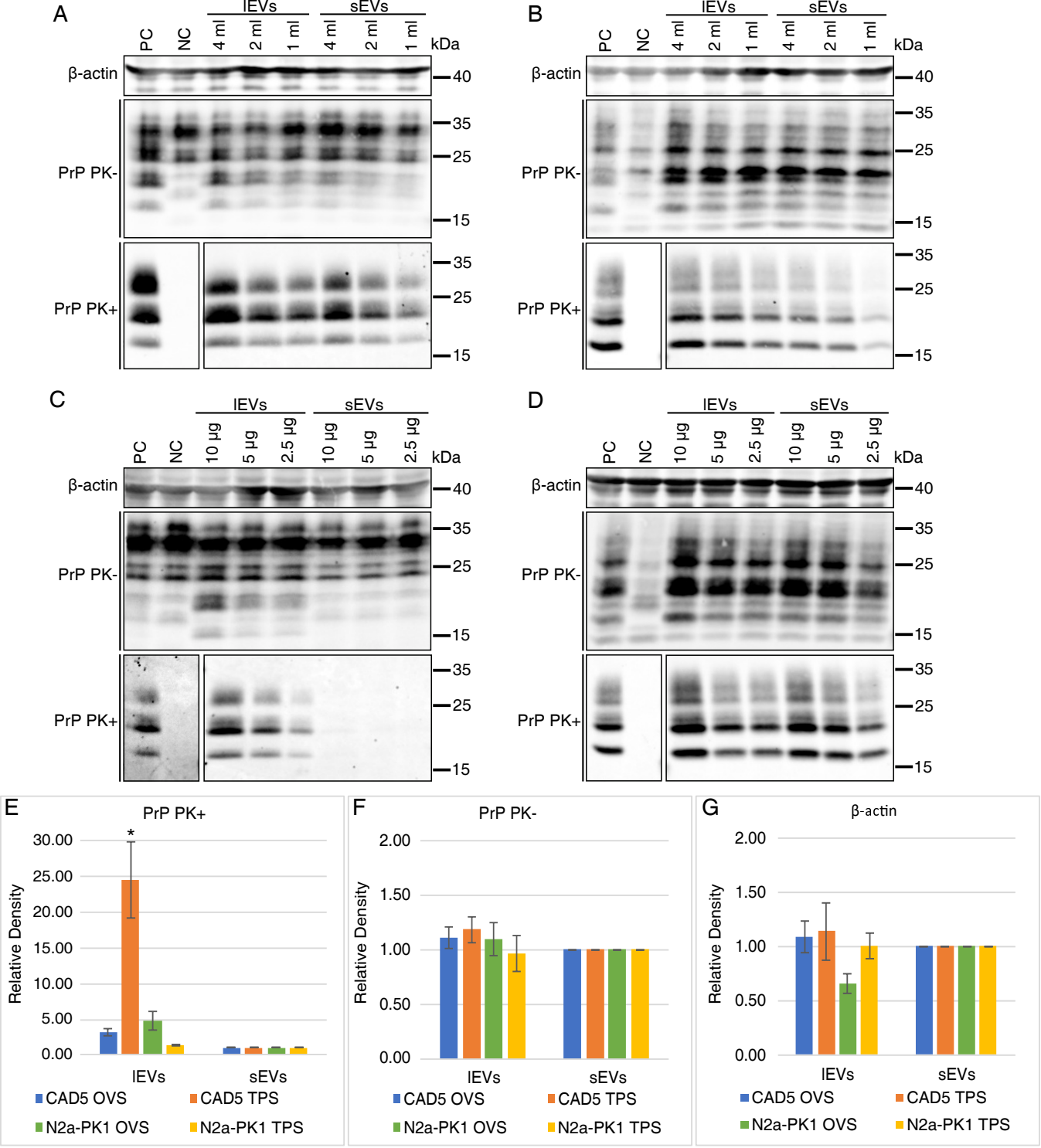
A
lEVs
sEVs
PC
NC
4 ml
2 ml
1 ml
4 ml
2 ml
1 ml
kDa
β-actin
PrP PK-
PrP PK+
40
35
25
15
B
C
10 µg
5 µg
2.5 µg
D
E
PrP PK+
Relative Density
30.00
25.00
20.00
15.00
10.00
5.00
0.00
*
CAD5 OVS
CAD5 TPS
N2a-PK1 OVS
N2a-PK1 TPS
F
PrP PK-
2.00
1.50
1.00
0.50
0.00
G
β-actin

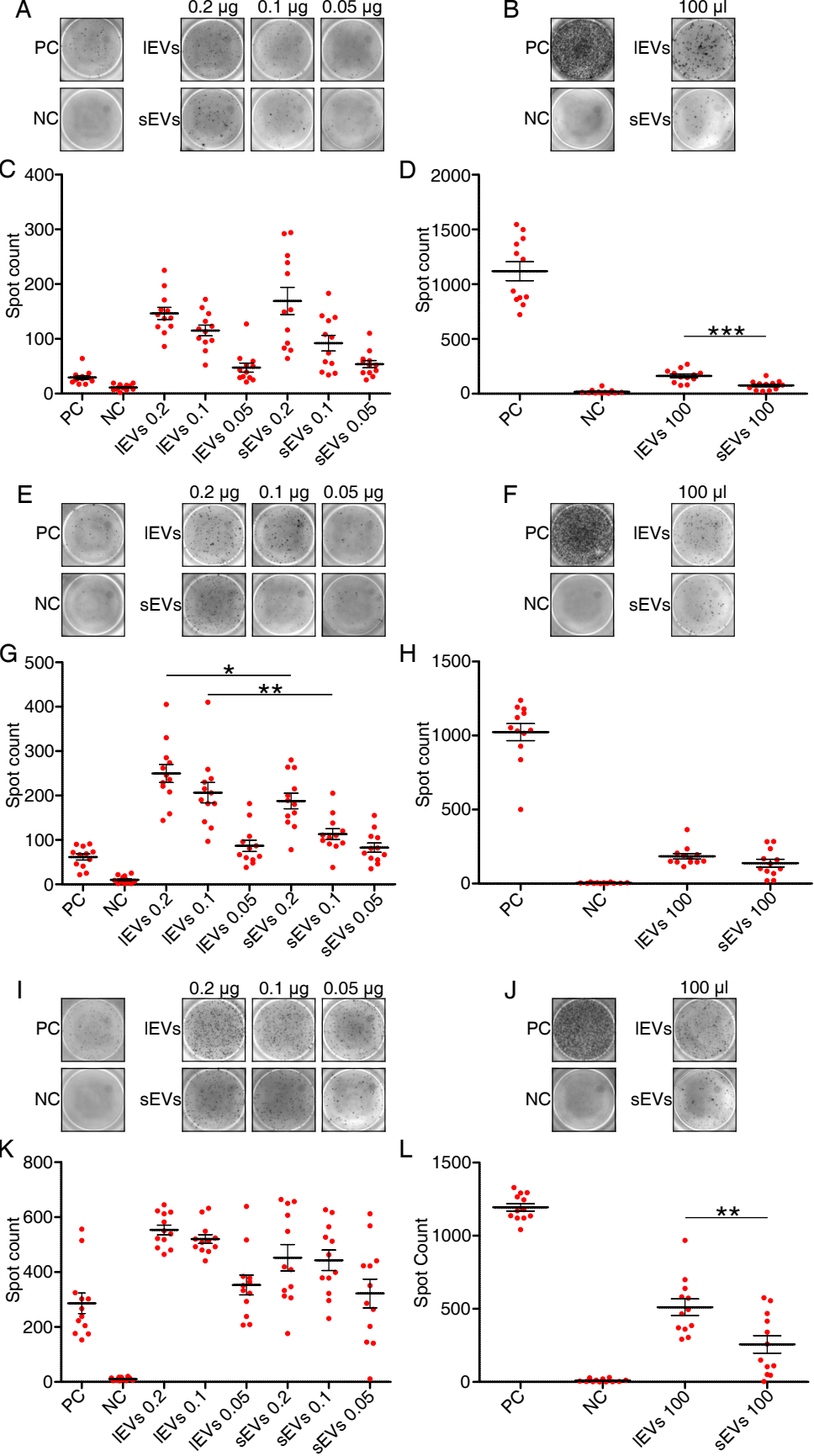
A
0.2 µg
0.1 µg
0.05 µg
PC
lEVs
NC
sEVs
B
100 µl
C
Spot count
PC
NC
lEVs 0.2
lEVs 0.1
lEVs 0.05
sEVs 0.2
sEVs 0.1
sEVs 0.05
D
***
lEVs 100
sEVs 100
E
F
G
*
**
H
I
J
K
L
Spot Count